https://ntrs.nasa.gov/search.jsp?R=19670008827 2020-03-16T18:57:02+00:00Z

TECH LIBRARY KAFB, NM
0061177

NASA CONTRACTOR REPORT

N.A.S.A.-C.R.

NASA CR-678

LOAN COPY: RETURN TO
AFWL (WLIL-2)
KIRTLAND AFB, N MEX

HEAT TRANSFER TO CRYOGENIC HYDROGEN FLOWING TURBULENTLY IN STRAIGHT AND CURVED TUBES AT HIGH HEAT FLUXES

Prepared by
AEROJET-GENERAL CORPORATION
Sacramento, Calif.
for Western Operations Office

NATIONAL AERONAUTICS AND SPACE ADMINISTRATION • WASHINGTON, D. C. • FEBRUARY 1967

TECH LIBRARY KAFB, NM
0060177

NASA CR-678

HEAT TRANSFER TO CRYOGENIC HYDROGEN FLOWING TURBULENTLY IN STRAIGHT AND CURVED TUBES AT HIGH HEAT FLUXES

Distribution of this report is provided in the interest of information exchange. Responsibility for the contents resides in the author or organization that prepared it.

Prepared under Contract No. SNPC-35 by
AEROJET-GENERAL CORPORATION
Sacramento, Calif.

for Western Operations Office

NATIONAL AERONAUTICS AND SPACE ADMINISTRATION

For sale by the Clearinghouse for Federal Scientific and Technical Information
Springfield, Virginia 22151 – Price $3.00

TABLE OF CONTENTS

TABLE OF CONTENTS, CONTINUED

LIST OF FIGURES

LIST OF TABLES

I. SUMMARY

The forced-convection heat-transfer characteristics of cryogenic hydrogen were studied in straight and curved tubes at pressures ranging from 800 to 1500 psi and fluxes from 8 to 27 Btu/in.^{2}-sec. The tests were conducted under conditions simulating those predicted for the Phoebus-2 nozzle, in support of the nozzle development program, and the test data were compared with the Hess and Kunz film-temperature equation. This equation, with a modified coefficient, represented both the straight and curved-tube test data. The dependency of the coefficient in terms of coolant temperature and geometrical configuration (i.e., radius of curvature and angular distance for curved tubes) was empirically evaluated, and the selection of a variable C_L as a multiplying factor for modifying the coefficient in the straight and curved portions of the nozzle, respectively, was substantiated.

II. INTRODUCTION

In designing a convectively-cooled nozzle for a nuclear rocket, the hot gas-side and the liquid (or coolant)-side heat transfer coefficients must be known to permit optimization of the coolant passage and an estimate of the pressure drop and coolant-temperature rise through the nozzle. The design of the nozzle for the higher power reactor design established a need for new technology and an extension of knowledge in many areas. Analysis predicted that the Phoebus-2 nozzle would be subjected to fluxes of 20 Btu/in.^{2}-sec and surface temperatures of 1600°F. The adequacy of the existing design equations for predicting the coolant-side heat transfer coefficient needed substantiation; this included an experimental evaluation of the ability of cryogenic hydrogen to accommodate heat fluxes in excess of 20 Btu/in.^{2}-sec the influence of throat radii of curvature on heat transfer, and possible adverse effects of low coolant temperatures on the heat transfer coefficient for the pressure range of interest.

A. PREVIOUS INVESTIGATORS

In the last few years basic experimental measurements of forced-convection heat transfer to hydrogen at supercritical pressures in straight, circular-cross-section tubes have been made. The regions of interest were pressures from 500 to 2500 psia, and coolant temperatures from 60°R to 200°R. Hendricks, Simoneau, and Friedman, (Ref. 1) studied the heat transfer characteristics of cryogenic hydrogen in uniformly heated tubes at pressures from 1000 to 2500 psi, and Miller, Seader, and Trebes (Ref. 2) published experimental test data for pressures ranging from 400 to 2500 psia. Both studies covered the pressure and temperature regime of specific interest, and the latter study included results at high heat fluxes.

The results of Hendricks, et al, for heated length-to-diameter ratios greater than 19, were satisfactorily compared with the Nusselt film temperature equation:

$$Nu_f = 0.021 \left(\frac{D\rho_f V_b}{\mu_f}\right)^{0.8} Pr_f^{0.4} \qquad (1)$$

where:

$$T_f = \frac{(T_w + T_b)}{2}$$

Miller, Seader, and Trebes in Reference (2) compared the data of Reference (3) with the Hess and Kunz equation as proposed in Reference (4). Re-examination of the data led to the selection of this same equation format, but revised the reference temperature and modified the coefficients as follows:

$$Nu_{0.4} = 0.0204 \left(\frac{\rho_{0.4} V_b D}{\mu_{0.4}}\right)^{0.8} Pr_{0.4}^{0.4} \left(1 + 0.00983\, \nu_w/\nu_b\right) \qquad (2)$$

The conclusions reached by Seader, et al, were that the Nusselt film temperature equation would be ultra-conservative at high heat fluxes at low coolant temperatures,

and that the additional correction factor of the ratio of the kinematic viscosities greatly improves the predictions of the simpler Equation (1).

An exhaustive analysis of hydrogen heat-transfer data in Reference (5) also concluded that the most representative equation was one incorporating a corrective kinematic viscosity ratio; however, an additional variable coefficient (or C_L, which is a function of the local coolant temperature) was used to characterize the test data. In this analysis the following equation was recommended for the pressure range 600 to 1500 psia:

$$Nu_f = 0.0208\ C_L\ Re_f^{0.8}\ Pr_f^{0.4}\ (1 + 0.01457\ \nu_w/\nu_b). \qquad (3)$$

This equation is the Hess and Kunz equation (Ref. 4) with a C_L term. The magnitude of the C_L term varies with coolant temperature $C_L = f\ (T_b)$ for straight and curved tubes as follows:

	C_L	
Coolant Temp., °R	Straight Tube	Curved Tube
50	2.0	
55	1.73	
60	1.48	1.95
65	1.26	1.64
70	1.07	1.37
75	.93	1.21
80	.87	1.11
85	.85	1.10

Analysis of the Phoebus-2 nozzle was performed, based on the use of a C_L value of 0.85 for all straight portions of the nozzle and 1.0 for the curved-tube portion corresponding to the throat region of the nozzle. From this analysis it was determined that the heat flux in the nozzle throat would be 20 Btu/in.^{2}-sec and the gas-side wall temperature would be 1600°F. Therefore, an experimental investigation

of the local heat-transfer pressure-drop behavior of cryogenic hydrogen in straight, electrically heated tubes at heat fluxes up to 25 Btu/in.^{2}-sec was conducted.

A significant difference was noted between the heat-transfer coefficient on the concave (outside) and the convex (inside) surfaces in a curved tube. This behavior was studied by Hendricks and Simon, Reference (6), for sub-critical (two-phase) liquid, supercritical liquid, and gaseous hydrogen in symmetrically heated curved tubes. From this study the magnitude of the variation in heat transfer between the concave and convex sides and the influence of angular distance around the curve were found to be influenced by the fluid temperature and the radius of curvature. In a previous study, Reference (7), the improvement of heat transfer in curved tubes with non-uniform (or asymmetric) heating was studied in basically one-tube geometry. Neither of these studies resulted in a relationship permitting ready extrapolation to other design conditions; hence, additional design data were needed, specific to the configuration envisioned for the Phoebus-2 nozzle.

Ito, Reference (8), studied the presssure drop for flow in curved tubes and found that the increase in resistance to flow around a curved-flow passage could be computed from the relationship:

$$f_c/f_s = \left[\mathrm{Re}(r/R)^2\right]^{0.05} \qquad (4)$$

where:

f_c/f_s = ratio of flow resistance in curved tube to straight tube.
Re = Reynolds number
r = Tube radius
R = Radius of curvature

Based on Reynolds' analogy, an increase in resistance to flow should be accompanied by an increase in heat transfer, and Equation (4) could be used to predict the

overall increase in heat transfer. This relationship does not, however, indicate how the heat-transfer coefficient would vary around the curve, nor can one infer possible effects introduced by non-circular cross-section flow paths. A series of curved-tube tests was, therefore, conducted to determine the magnitude of enhancement to heat transfer on the outside (concave) surface of the curve in asymmetrically heated tubes with two different curvatures.

B. EXPERIMENTAL PROGRAM

The test program consisted of a series of tests conducted in two types of electrically heated Hastelloy X tubes: (1) straight tubes of uniform wall thickness, and (2) curved tubes of non-uniform wall thickness (designed to simulate two different nozzle throat geometries). The test conditions of the current program were, therefore, selected to simulate as nearly as possible the predicted conditions in the nozzle, minimizing the need for extrapolation.

III. DESIGN OF EXPERIMENT

The tests conducted in this experimental program were designed to simulate predicted test conditions in the coolant passage of the Phoebus-2 Nozzle and/or the coolant-passage configuration. Test sections were fabricated from Hastelloy X tubing. Tests were conducted at coolant pressures of 800-1500 psi with instrumentation to measure pressure drop across the test section, coolant flow rate, electrical-energy input, sensible-energy rise, and tube-wall temperature. From these measurements the coolant-side wall temperature, local heat flux at the liquid-metal interface, local coolant temperature, and local heat-transfer coefficient were determined.

A. SCOPE OF INVESTIGATION

The range of the test conditions achieved in these tests are tabulated in Tables 1 and 2 for the straight and the curved-tube tests, respectively. There were two objectives of the straight-tube tests: to study the effects of coolant temperatures near the transposed critical temperature on the local heat-transfer coefficient, and to demonstrate that heat fluxes in excess of 20 Btu/in.^{2}-sec can be sustained. The curved-tube tests were to determine the degree of enhancement caused by tube curvature, and the persistence of any enhancement around the curve.

B. TEST SECTION DESIGN

Only Hastelloy X tubing was used in these experiments. Initially, the test sections were prepared by torch-brazing copper electrodes onto the tubing with silver-solder. Later in the program the procedure was altered to one of furnace brazing the electrodes to the tubing using NIORO braze material in a hydrogen atmosphere. A length of tubing extended upstream of the heated length served as a hydraulic stabilizing section. Pressure taps were located in or near the copper electrodes for direct measurement of pressure drop across the heated length. Outer-tube wall temperatures and local voltage drops were measured at stations along the heated length by instrumenting the external surface between the electrodes with fine-wire (No. 40 gauge chromel-alumel) thermocouples and voltage taps. Each thermocouple junction was electrically insulated from the current-carrying tube by a thin layer of mica (0.0005-to 0.001-in. thick) and was held in place mechanically by a wrapping of glass rovings and (on the curved tubes) included a stainless-steel wire binding.

1. Straight Tubes

The sections tested in the straight-tube portion of the test program were tubes of 3- and 6-inch heated lengths, as shown by Figure 1. Four thermocouples were affixed to the short tubes and eight to the long tubes. Tube diameter was limited by the test durations desired and the associated mass velocities. A reduced tubing diameter resulted in a reduced test-section length to achieve the best impedance match between the test section and the power supply, permitting attainment of the highest possible heat fluxes.

TABLE 1

RANGE OF STRAIGHT-TUBE TEST PARAMETERS

Parameter	Range
D_i, in.	0.147
L_{heated}/Di	6.6-33.9
P_b, psia	696-1371
T_b, °R	61.6-96.8
T_w, °R	430-1681
G, lbm/ft^2-sec	596-3583
V, ft/sec	166-1534
Q/A, $Btu/in.^2$-sec	6.4-27.6

TABLE 2

RANGE OF CURVED-TUBE TEST PARAMETERS

Parameter	CAC* 4-8	CAN** 4-8	CAC 2-4	CAN 2-4
DRAD, in.	4.00	5.50	2.00	2.45
URAD, in.	8.00	8.80	4.00	4.00
De, in.	0.214	0.195	0.214	0.195
L_{heated}/De	21.0-67.7	23-69	23.3-46.7	25.6-51.1
P_b, psia	850-1256	1088-1259	892-1178	865-1230
T_b, °R	65-94	79-130	72-112	70-109
T_w, °R	195-1641	406-1348	262-1603	168-1071
G, lbm/ft^2-sec	1186-1832	860-978	796-1533	981-1691
Q/A, $Btu/in.^2$-sec	7.4-12.4	7.2-12.5	6.4-12.9	7.0-12.9
V, ft/sec	323-694	258-558	277-606	302-689

*Curved-Asymmetrically Heated, Circular Cross-Section
**Curved-Asymmetrically Heated, Non-Circular Cross-Section

Straight-Tube Test-Section Schematic

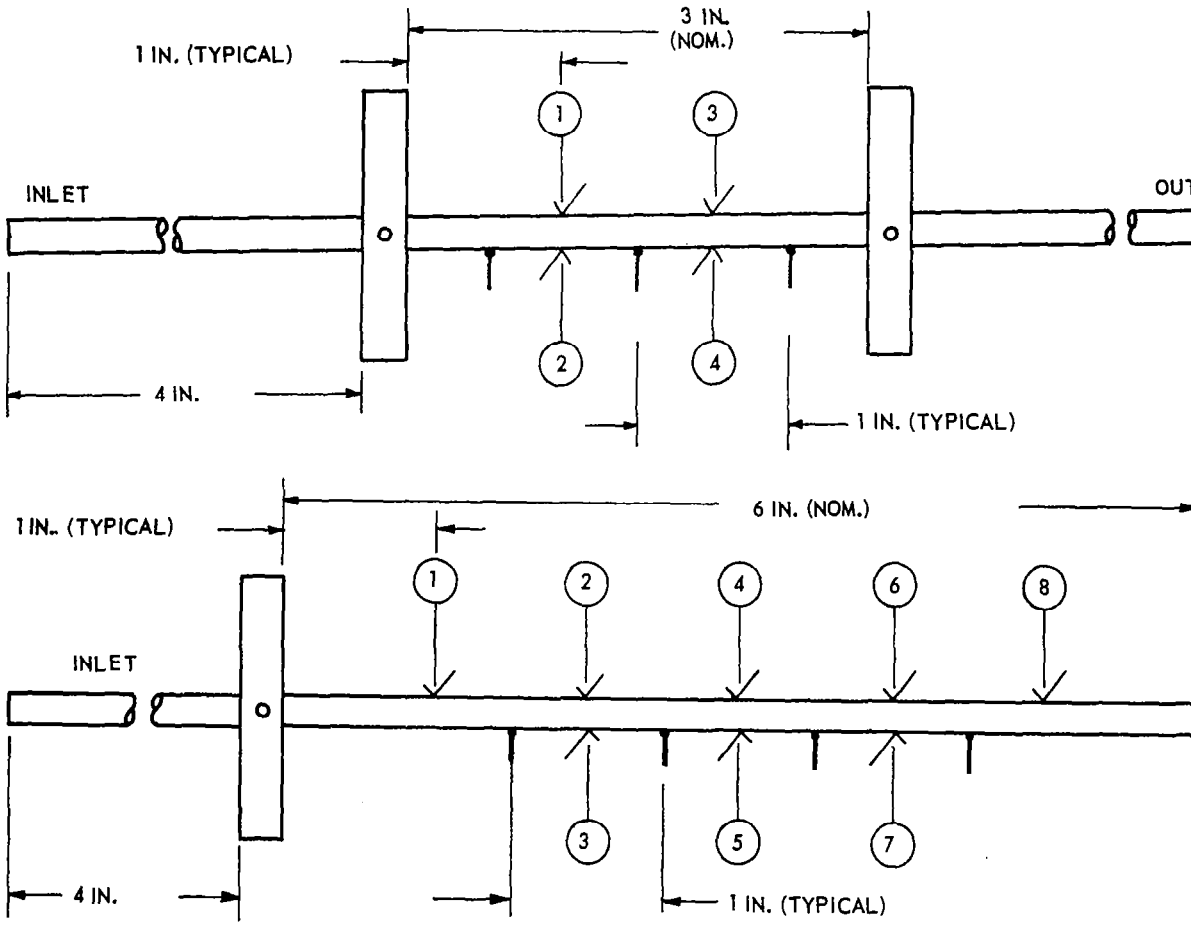

0.147-IN. INSIDE DIAMETER X 0.020-IN.-WALL THICKNESS
HASTELLOY X TUBING

Figure 1

2. Curved Tubes

Curved-tube test sections were fabricated from 5/16-in. x 0.049-in. wall thickness tubing. The tubes were bent with two radii of curvature to simulate the throat region in a rocket nozzle, as shown by Figure 2. A straight section preceded the curved portion corresponding to the skirt region of the nozzle and served as a pre-heater section, conditioning the fluid to the desired bulk temperature at the start of the curved portion of the tube. The compound bend consisted of a section bent through a 17-degree angle at a radius of curvature corresponding to the DRAD (downstream radius with respect to the gas flow in a rocket nozzle), followed by a section bent through a 45-degree angle at a radius corresponding to the URAD (upstream radius). The DRAD-URAD combinations selected for testing were nominal Phoebus-2 design radii of 4.0 and 8.0-in., respectively, and a second design of 2.0 and 4.0-in. (which is one half the Phoebus-2 design and approximates the NERVA nozzle geometry). The heated lengths of the two test sections were approximately 14 and 11 inches for the Phoebus-2 and NERVA design cases, respectively. One each of the small radii (2-4) and the large radii (4-8) test sections had a circular cross-section with a crown radius of 0.107-in. while a second similar pair were flattened to give a crown radius of 0.076-in. The sections were fabricated by bending, flattening, and finally chemical milling to the contour noted in Figure 2. By varying the tube-wall thickness it is possible to change the distribution of current flowing in the tube wall and, therefore, the local heat generation. In a non-uniform wall-thickness tube the local heat generated in the tube is proportional to the wall thickness (assuming a constant value of resistivity); for these tests the wall-thickness ratio was approximately 3:1. The thick wall (or high temperature side) of the tube was located on the outside of the bend (corresponding to the heated side in a nozzle), while the thin wall (or back side) of the tube remained at a relatively low temperature. The circular and non-circular tubes were designed to have the same high-heat-flux area and, by achieving the same test conditions, permit a direct comparison of test results between the different test sections. Wall-temperature measurements were made only on the crown, or as near the crown and axis of symmetry of the tube as possible, and not on the thin back-side of the tube.

Curved-Tube Test-Section Schematic

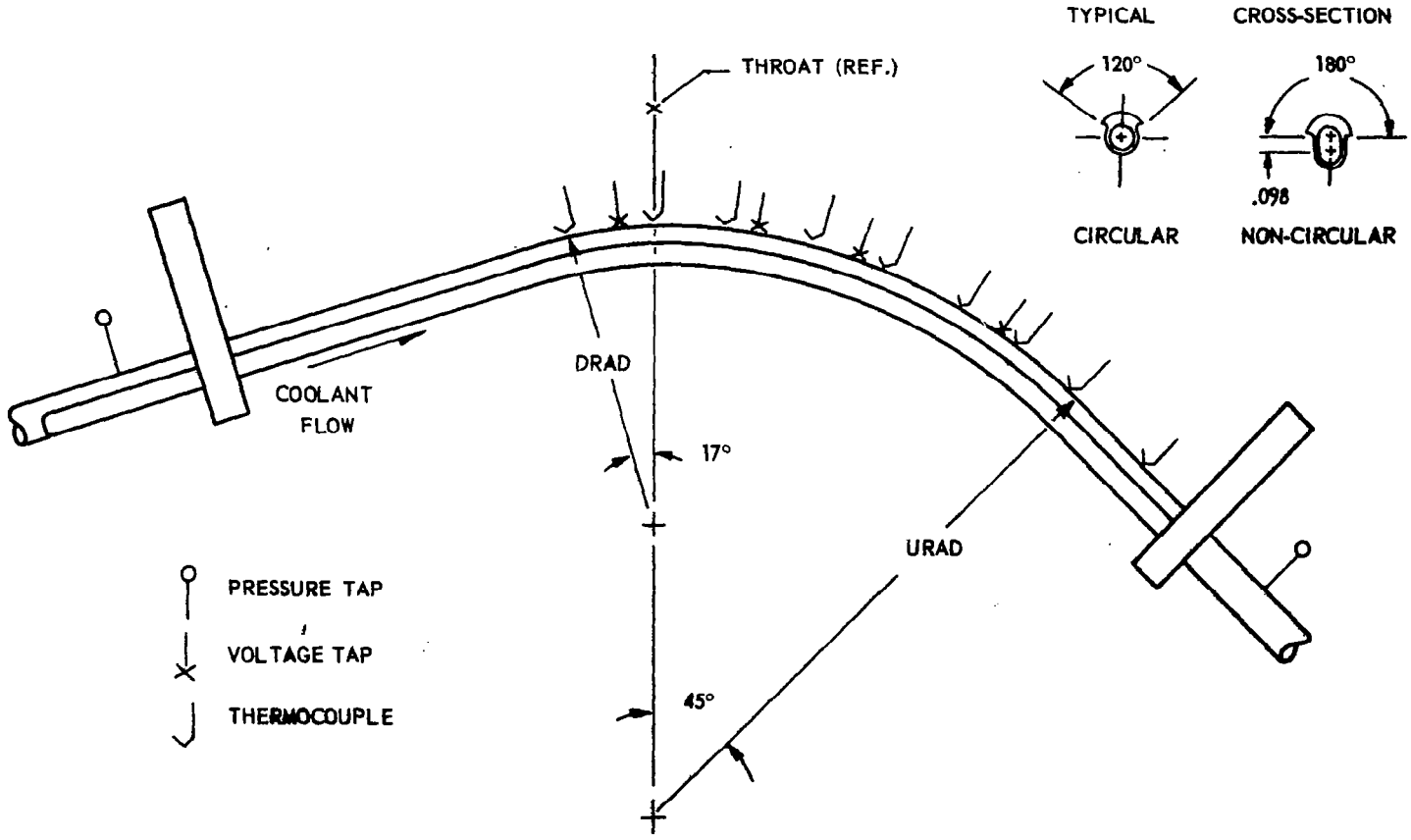

Figure 2

Reference (7) includes some data which indicate the magnitude of the heat flux measured on the thin back-side and also the temperature distribution around the crown of a curved asymmetrically-heated tube. The location of the instrumentation for the curved test sections is included in Table 3.

C. EXPERIMENTAL APPARATUS

Experimental heat transfer tests were started in a single-pass, gas-pressurized, blow-down loop located at the Aerojet-General test facility in Azusa. This facility included a 50-gallon vacuum-jacketed vessel, designed for a working pressure of 2200 psi. The instrumented test section and flow system was located in an evacuated enclosure, or "bonnet", directly over the run tank. A complete description of the facility is included in Reference (7). The latter portion of the straight-tube test program and the curved-tube tests were conducted at the Aerojet-General Sacramento Plant in the Physics and Chemistry Laboratory. Figure 3 is a sketch of the test apparatus associated with the high-pressure 130-gallon capacity blow-down loop at this facility. The run tank was a foam-insulated vessel designed for a working pressure of 3000 psi. The liquid was expelled from the run tank (by gaseous hydrogen) and through a metering orifice, the inlet mixing chamber, the test section, the outlet mixing chamber, a flow-control valve, and a vent to the atmosphere. The flow system and heat-transfer test sections were housed in an enclosure which maintained a helium atmosphere at a pressure of approximately 5 psi. The flow rate of the coolant was measured by a sharp-edged orifice, and was controlled by regulating the tank pressure and a motor-operated flow-control valve in the vent line. Coolant temperature was measured with platinum reistance thermometers; pressures were sensed by variable-reluctance pressure transducers insulated electrically from the test section and isolated from the flow system by long gas legs. Fluid temperatures and pressures were measured in mixing chambers.

TABLE 3

CURVED-TUBE TEST-SECTION GEOMETRY

Test No.	Test Section	Crown Radius (in.) Outside/Inside		DRAD (in.)	URAD (in.)	Thermocouple Station Distance From Inlet Electrode (in.) 1	2	3	4	5	6	7	8	9
HT-3-116	CAC* 408	.312	.107	4.00	8.00	4.5	5.5	6.5	7.5	8.5	9.5	10.5	11.5	14.2
HT-3-118	CAC 2-4	.312	.107	2.00	4.00	5.0	5.5	6.0	6.5	7.0	7.5	8.0	9.0	10.0
HT-3-119, -120	CAN** 2-4	.25	.076	2.45	4.00	5.0	5.5	6.0	6.5	7.0	7.5	8.0	9.0	10.0
HT-3-121	CAN 4-8	.25	.076	5.50	8.80	4.5	6.0	6.5	7.5	8.5	9.5	11.0	12.5	13.5

Test No.	Total Heated Length (in.)	Voltage Tap Distance from Inlet (in.) A	B	C	D	Upstream Point of Tangency Distance from Inlet (in.)
HT-3-116	14.70	5.25	6.75	8.23	10.25	5.0
HT-3-118	11.57	2.63	5.25	6.75	8.75	5.0
HT-3-119, -120	10.87	2.63	5.25	6.75	8.77	5.1
HT-3-121	14.0	5.50	7.00	9.00	11.75	4.5

*Curved-Asymmetrically Heated, Circular Cross-Section
**Curved-Asymmetrically Heated, Non-Circular Cross-Section

Test-Section-Assembly Liquid-Hydrogen Heat-Transfer Apparatus

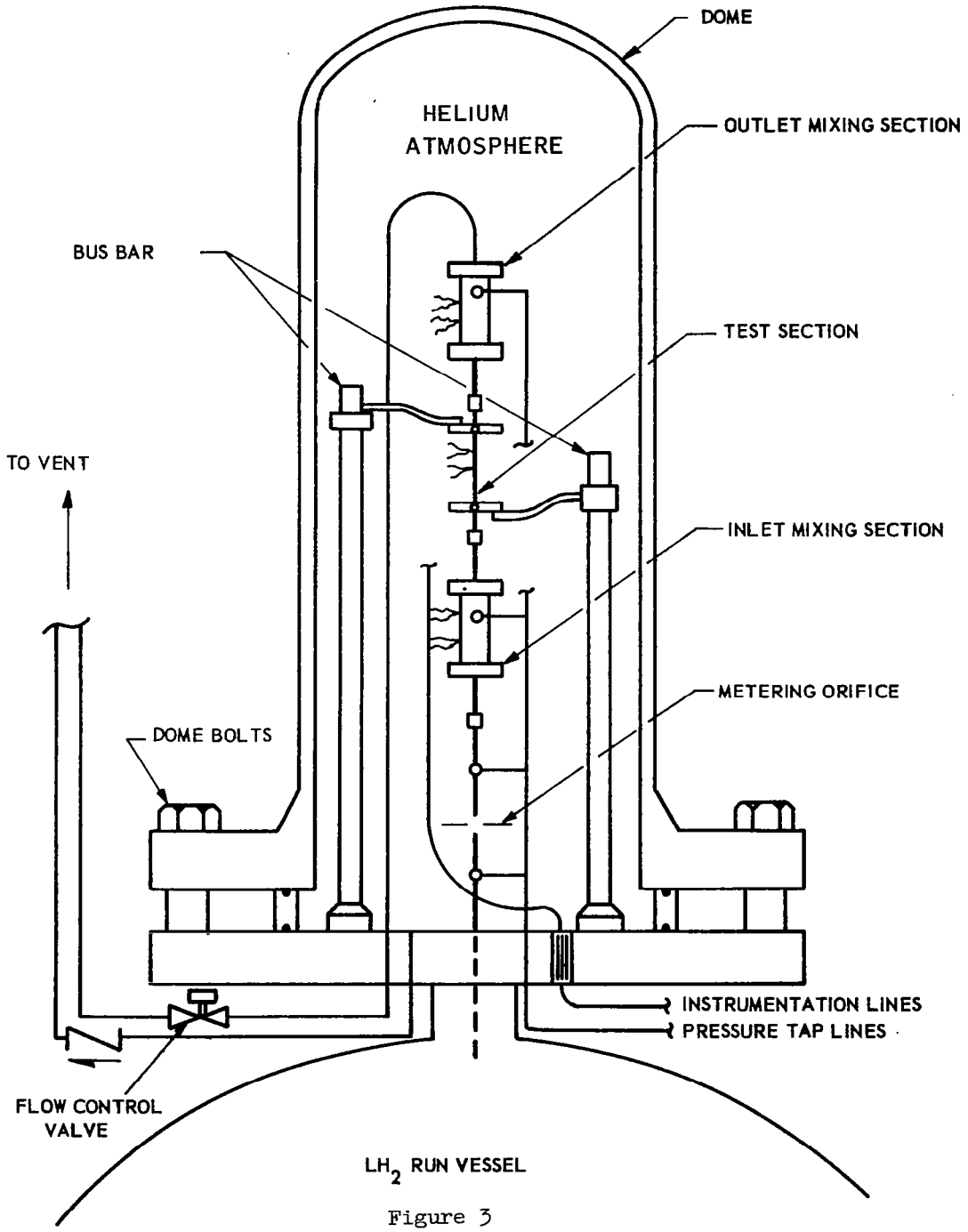

Figure 3

Test sections were resistance-heated by direct current supplied by four 15-volt, 3300-ampere, saturable-reactor-regulated ac rectifiers with a total capacity of 200 kw.

The measured test parameters, current, voltage, temperatures, and pressures were sampled at a sampling rate of 156 data points per second and recorded on magnetic tape. The data tape was input to a digital computer which averages the measurements over a prescribed interval (1-5 seconds), while at steady-state and tabulates the results, showing the time (from the start of the test) at which the data were sampled, the number of readings averaged, the average, and the maximum deviation (positive or negative) from the average.

IV. EXPERIMENTAL PROGRAM

A. TEST PROCEDURE

For each test section, runs were made from a few specific flow rates over a range of power levels. The test procedure consisted of filling the run tank with liquid hydrogen, securing the vent valve, pressurizing the tank to the desired test pressure, and opening the flow-control valve. The desired flow rate was established and power was applied to the test section. When power was increased, the fluid density decreased, reducing the flow rate through the flow-control valve. Since control of this valve was manual, either the valve was opened to maintain the desired flow, or the system pressure was increased. Complete expulsion of the test fluid was signalled by an increase in the inlet-coolant temperature, at which time the test was stopped.

B. DATA REDUCTION

Digital test data are recorded on tape and the recorded data for a period of 1 to 3 seconds are averaged. These data are entered as input to the IBM 7094 computer for data reduction. The computer program calculates the total input electrical power, the enthalpy rise of the test fluid, the fluid-flow rate, and the heat balance for each test condition. At each thermocouple station the local coolant pressure and temperature are computed, as are the temperature drop through the heated wall and the unit heat

flux at the hot-wall-fluid interface. Subsequently, the local heat-transfer coefficient and the fluid velocity are computed at this thermocouple station. Computation of the inner-wall temperature and heat flux is based on a finite-differences solution to the exact differential equation describing the flow of heat through an internal heat-generating solid with temperature-dependent properties of thermal conductivity and resistivity.

Coolant temperature and pressure at each thermocouple station are computed from the inlet and outlet-mixing-chamber temperatures and pressures. It is assumed that the flow is adiabatic from the inlet mixer to the start of the heated length, and from the outlet of the heated length to the outlet-mixer section. The pressure drop along the heated length of the test section is assumed to be linear, as is the rate of heat addition. The local coolant temperature is based on the computed static enthalpy along the heated length.

1. Fluid Properties

The fluid properties used in the reduction of the experimental test data are based on the PVT as well as thermodynamic and transport properties contained in a TAB code. Para-hydrogen properties are calculated from this TAB code from given data points using two-dimensional linear interpolation. The para-hydrogen property code (termed TAB T) covered the temperature and pressure range of 36 to 5000°R and 0-1500 psia and is described in Reference (9).

2. Energy Balance

An energy balance is the primary means of estimating the accuracy of the measured variables (current, voltage, coolant flow rate, coolant temperature, and coolant pressure). The electrical energy supplied to the test section (Q_p), is equal to the enthalpy change of the fluid (Q_s) plus any losses or gains, (Q_L):

$$Q_p = Q_s + Q_L$$

where

$$Q_p = 0.948\ EI \times 10^{-3}\ \text{Btu/sec}$$

$$Q_s = \dot{w}\left(\Delta H + \frac{V_{out}^2 - V_{in.}^2}{2\,g_c\,J}\right),\ \text{Btu/sec}$$

Q_I = losses or gains by conduction, convection, or radiation, Btu/sec

I = current, amperes

E = voltage drop across heated length, volts

$\dot{w}$ = flow rate, lb/sec

ΔH = enthalpy change, Btu/lb

In general, the energy balance, $(Q_p - Q_s)/Q_p$, was negative, indicating that the measured energy gain exceeded the electrical energy input.

The primary source of error in the experimental program was the mass-flow-rate measurement. The result of a systematic error in the measurement of the flow rate is cubed in computing the kinetic energy exchange, and any check on the heat balance is compounded by the lack of an actual coolant temperature measurement immediately at either the inlet and/or outlet of the heated length. In the first straight-tube tests this was not a significant problem because of relatively low fluid velocity. However, in subsequent high heat-flux tests the simplified approach to the calculation of the energy balance, ignoring entrance and exit effects, leads to a large apparent error in the heat balance. In the curved-tube tests the extreme changes in velocity were not encountered and the heat balances were generally within $\pm$ 10%.

3. Inner-Wall Temperature

The computation of a local heat-transfer coefficient requires a knowledge of the local heat flux and the local temperature potential, i.e., the local metal temperature less the local coolant temperature. Since inner-wall temperatures cannot be measured

directly, outer-wall temperatures must be measured and a computational technique devised to compute the temperature drop through the metal. In this program a finite differences solution of the equation for describing the steady-state two-dimensional thermal conduction of heat through a heat-generating solid with temperature-dependent properties was used to compute the inner-wall temperature. The solution of this equation required a knowledge of the tube axial-voltage gradient and the geometry (outside and inside radii). The electrical resistivity was input as a table which was curve-fit by a polynomial equation of four terms, while the conductivity was based on linear interpolation of tubular data. The data used in this program are tabulated in Table 4.

4. Local Coolant Temperature

Calculation of the local coolant temperature was based on the change in enthalpy of the test fluid from the test section inlet to that point on the test section where the outer-wall temperatures were measured. It was assumed that the electrical energy input was proportional to the tube length. Because of the large variation in velocity associated with the density change, the energy loss caused by the change in momentum was included in the calculation of the local coolant temperature.

5. Local Heat Flux

For a uniform wall thickness tube it is assumed that the current density is uniform and that the local and average heat fluxes are defined as the power input per unit area of wetted surface. However, for an asymmetrically heated tube, the current density is not uniform and the local and average heat fluxes are not equivalent; so the local heat flux must be determined. The heat fluxes computed in this program were based on the computed temperature gradient at the inner surface of the heated tube. For the curved-tube test sections the value of local heat flux reported is the computed flux along a line of symmetry of the tube.

TABLE 4

PROPERTIES OF HASTELLOY X

Temperature (°R)	Thermal Conductivity[1] (Btu/in.-sec-°R)	Temperature (°R)	Resistivity[2] (ohm/in. x 10^6)
190	1.01×10^4	600	48.05
200	1.02×10^4	750	48.60
250	1.03×10^4	950	49.35
300	1.06×10^4	1100	49.90
350	1.09×10^4	1300	50.65
400	1.12×10^4	1420	51.10
450	1.17×10^4	1600	51.70
500	1.23×10^4	1650	51.75
600	1.38×10^4	1750	51.61
800	1.67×10^4	1950	50.64
1000	1.96×10^4	2250	48.80
1200	2.25×10^4	2600	46.70
1400	2.54×10^4		
1600	2.83×10^4		
1800	3.12×10^4		
2000	3.41×10^4		
2200	3.70×10^4		
2400	3.99×10^4		
2600	4.28×10^4		
2800	4.57×10^4		
3000	4.86×10^4		

Data Source

(1) Figure 2.013 Aerospace Structural Materials Handbook, Vol II Non-Ferrous Alloys, ASD, USAF, (Revised Mar 1963)

(2) Ibid, Figure 2.022

6. Heat Transfer Coefficient

The local heat transfer coefficient was computed from the local heat flux and local thermal driving force

$$Q/A = h\ (T_w - T_b)$$

where:

Q/A=local heat flux, Btu/in.^{2}-sec

h =local heat transfer coefficient, Btu/in.^{2}-sec-^oR

T_w =local inner-wall temperature, ^oR

T_b =local coolant temperature, ^oR

7. Static Pressure

Pressure taps were located in the electrodes of the straight-tube test sections and 1.0-in. outside the electrodes on the curved-tube test sections. The local static pressure was computed, assuming a linear change in pressure along the heated length.

C. SPECIAL PROBLEMS

The measurement of the wall temperature of the curved-tube test section depends on the thermocouple being held in good thermal contact on the tube, while remaining electrically insulated from the tube. Mica was selected as the electrical insulator material because it maintains its electrical resistance at higher temperatures than most other insulators and it is easy to apply. In the performance of the curved-tube tests at high surface temperatures, the combined effect of the increase in electrical conductance of the mica and the voltage gradient in the tube apparently resulted in failure of the dc amplifiers in the thermocouple circuits. This condition resulted in loss of certain of the wall temperature data during the first two curved tube tests HT-3-116 and -117 and necessitated the repeat of test HT-3-117. The curved tube tests were originally designed to be conducted at heat fluxes of 15-18 Btu/in.^{2}-sec, and after this difficulty,were subsequently conducted at 12 Btu/in.^{2}-sec and below because of the outer wall temperature limitation. In addition,where a layer of mica 0.0005-in. thick

was used on the straight-tube tests, it was increased to 0.001-in. for the curved tube tests. The random failure of wall thermocouples persisted during the conduction of the tests and some thermocouples were lost on the straight portion of the tube at either the upstream or downstream straight position of the test section where the outer wall temperatures would be the highest. The affected thermocouple data have been deleted from the tabulation of curved tube test data in Appendix B.

V. RESULTS OF DISCUSSION

A. SUMMARY OF TEST PARAMETERS

The heat transfer tests were conducted in tubular Hastelloy X test sections. The straight-tube tests were conducted in two groups, one series of tests in 3-in. heated length tubes to generate high wall temperatures at low coolant temperatures and another series of tests in 3- and 6-in. heated length tubes to generate test data at high heat fluxes.

Tests to determine the effect of geometry on heat transfer were conducted in curved tubes of uniform flow area and asymmetric heat addition. Two different curvatures were studied with both circular and non-circular cross-sections, to more closely simulate the actual nozzle geometry.

Test data for the straight-tube tests are included in Appendix A, and for the curved-tube tests as Appendix B.

B. PREDICTION OF HEAT TRANSFER

Several equations were proposed for correlating hydrogen heat transfer data. The validity of any of these equations to adequately predict the heat transfer coefficient can be tested by comparing the test data with each equation. In this program two proposed equations were compared with themselves and with the straight tube data. The equations compared are the Nusselt film temperature equation and the Hess and Kunz equation with a modified coefficient. Both equations are based on film temperature

properties, or an arithmetic mean temperature between the wall and film temperature. The comparison of these equations for pressures of 800, 1200, and 1500 psia are shown by Figures 4, 5, and 6. In each figure the equations are ratioed and the ratio is plotted as a function of coolant temperature for lines of constant wall temperature. The range of coolant temperature is 50 to 140°R, and the wall temperature is from 400 to 1500°R. The following conclusions can be drawn from this comparison:

a. The variation between the two equations is less than ± 20% at wall temperatures below 800°R.

b. Increasing pressure reduces the difference between the two equations.

c. The difference in the predicted coefficients decreases for increasing coolant temperatures at higher wall temperatures.

d. The largest deviation between the two predictions occurs at coolant temperatures between 80-100°R at pressures of 800 psia and decreases with increasing pressure.

1. Straight Tube Test Data

In this particular study the deviation of the equations at high wall temperatures in the coolant-temperature regime (70-100°R) was the region of particular interest. The comparison of test data for different wall temperature regimes with the Nusselt film temperature equation is shown by Figures 7, 8, and 9 and the same data are compared with the Hess and Kunz equation by Figures 10, 11, and 12. In general, the Nusselt film temperature understates the coefficients by 20 to 25%, whereas the modified Hess and Kunz equation represents a less pessimistic representation.

Comparison of Predictive Equations for LH_2 at 800 psia

$$h = 0.021\ Re_f^{0.8}\ Pr_f^{0.4}\ k_{f/D}$$

$$h_c = 0.0176\ Re_f^{0.8}\ Pr_f^{0.4}\ (1 + 0.01457\ \nu_w / \nu_b)\ k_{f/D}$$

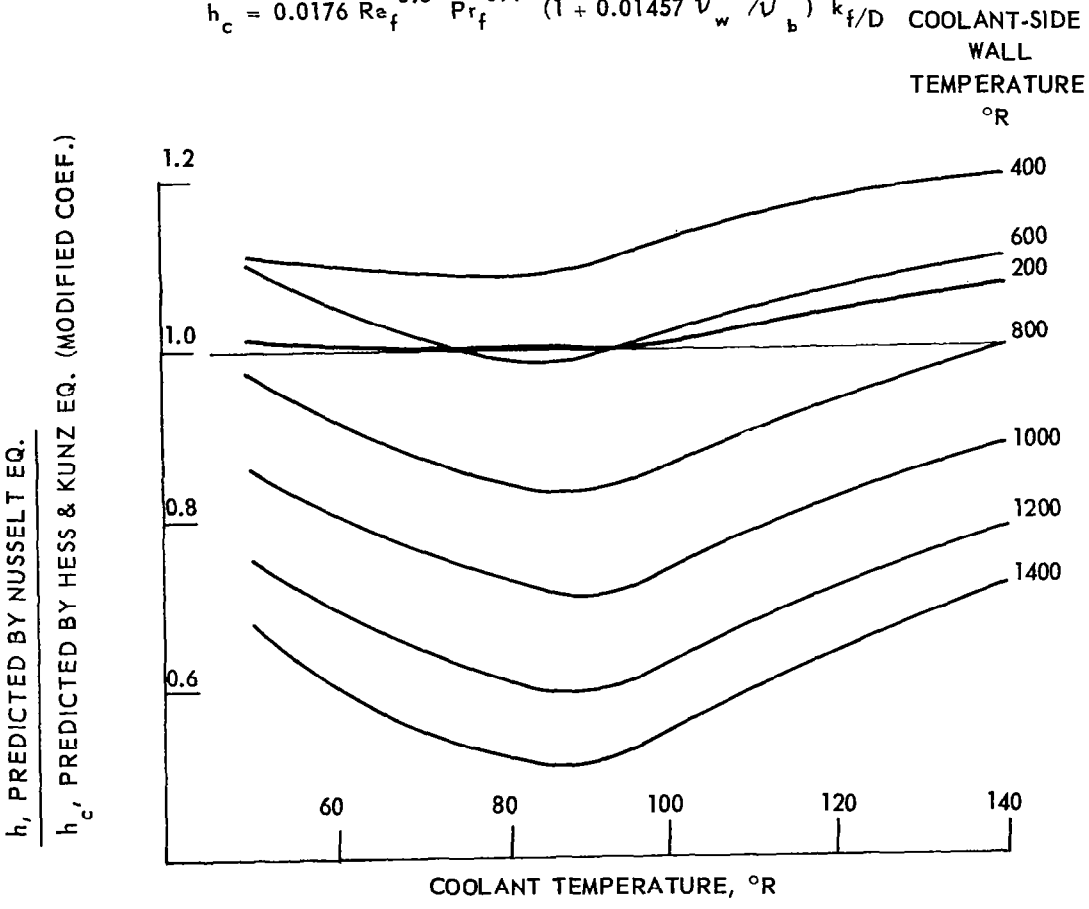

Figure 4

Comparison of Predictive Equations for LH_2 at 1200 psia

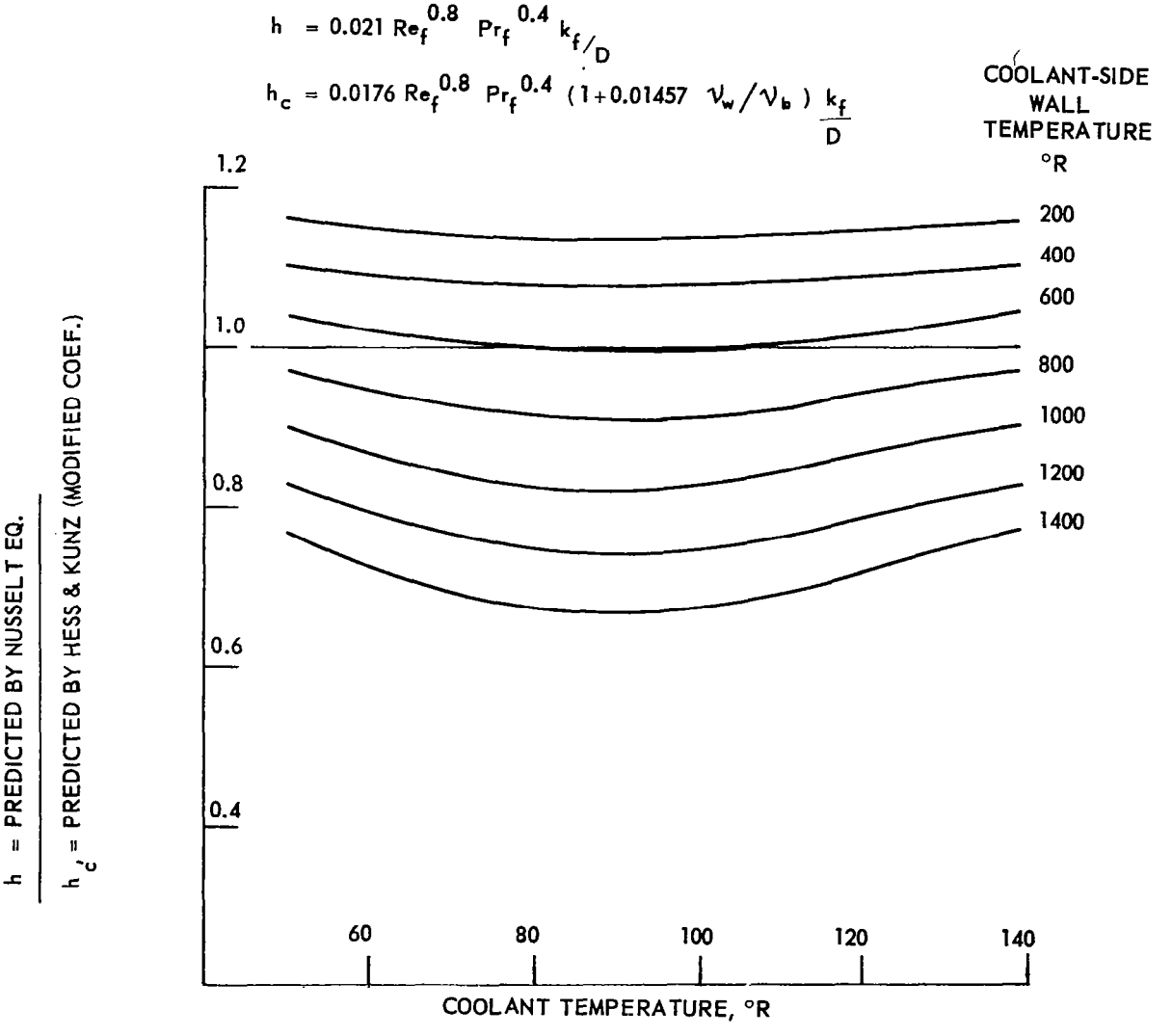

Figure 5

Comparison of Predictive Equations for LH_2 at 1500 psia

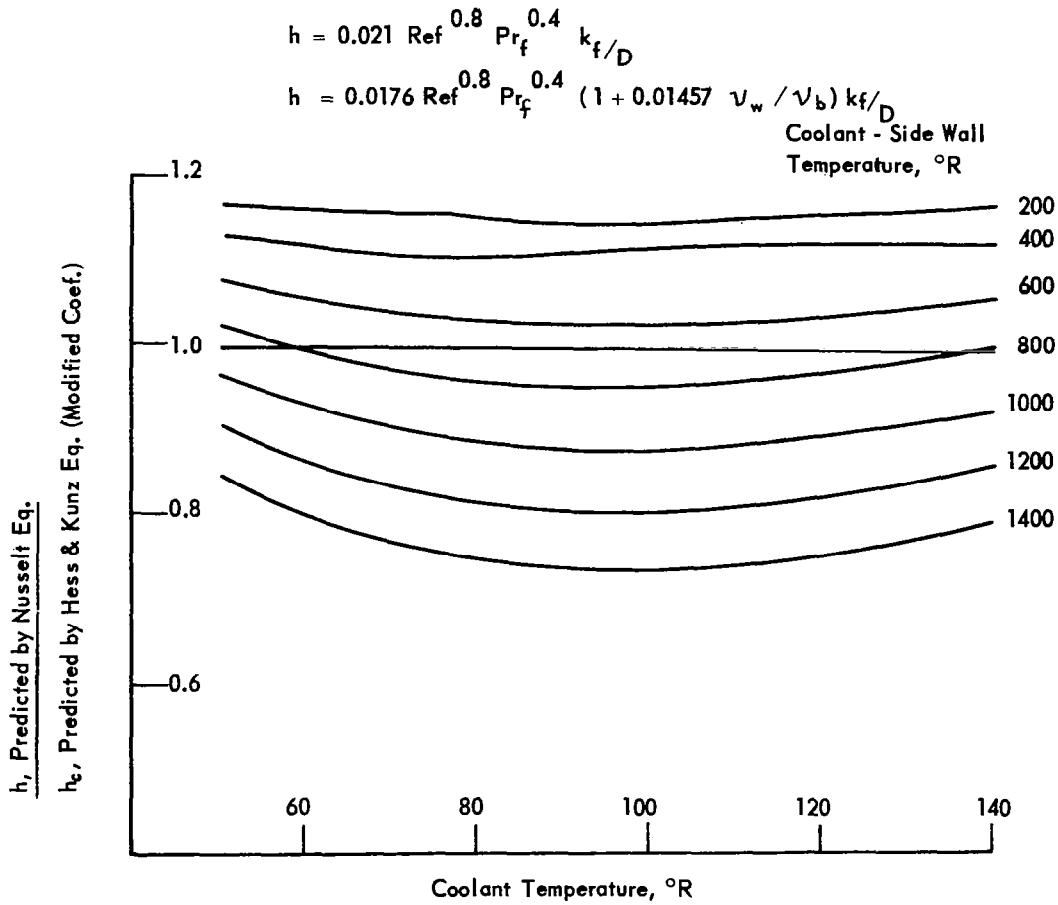

Figure 6

800 to 1000°R Wall-Temparature Data Compared with Nusselt Equation

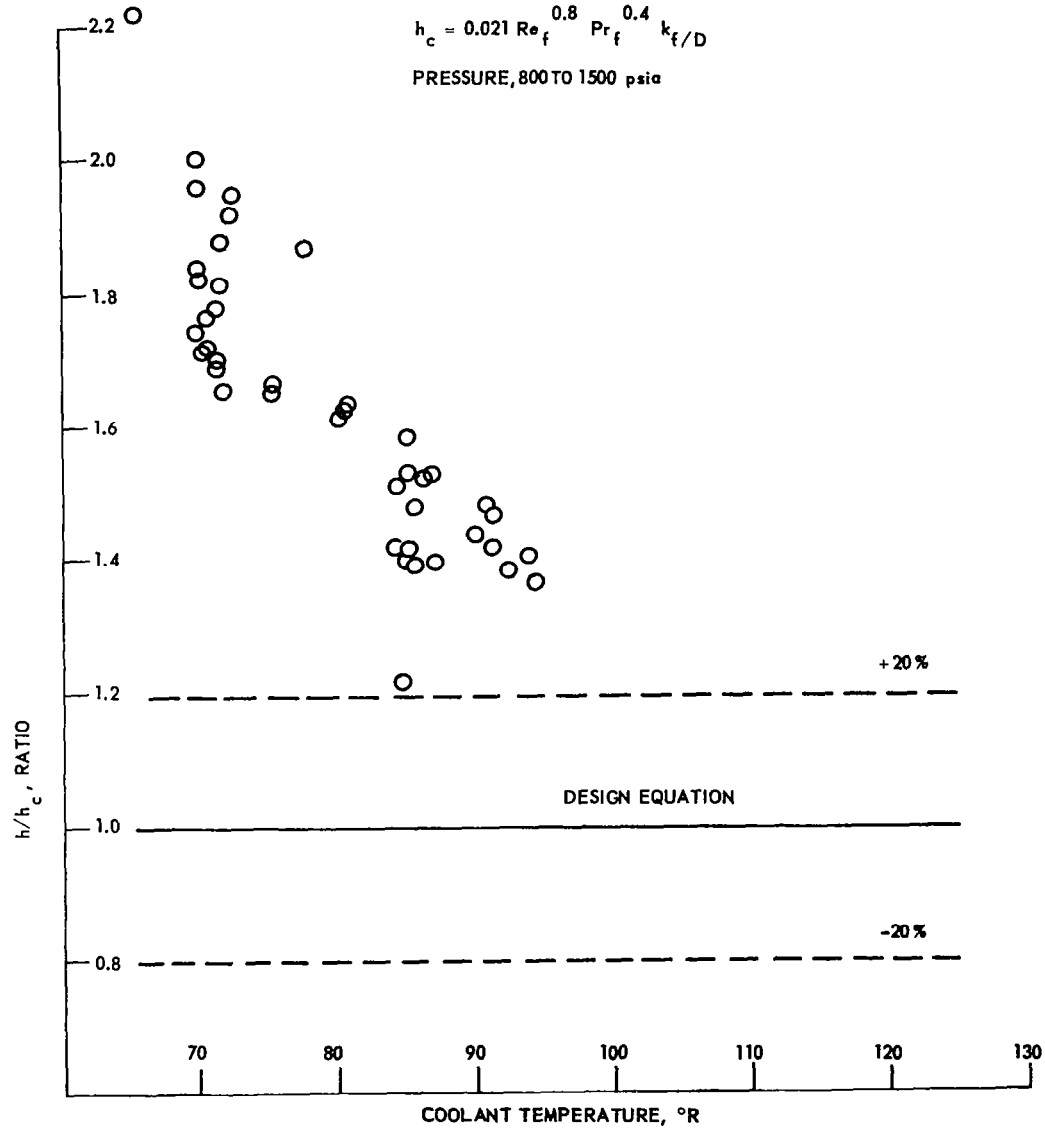

Figure 7

1000 to 1200°R Wall-Temperature Data Compared with Nusselt Equation

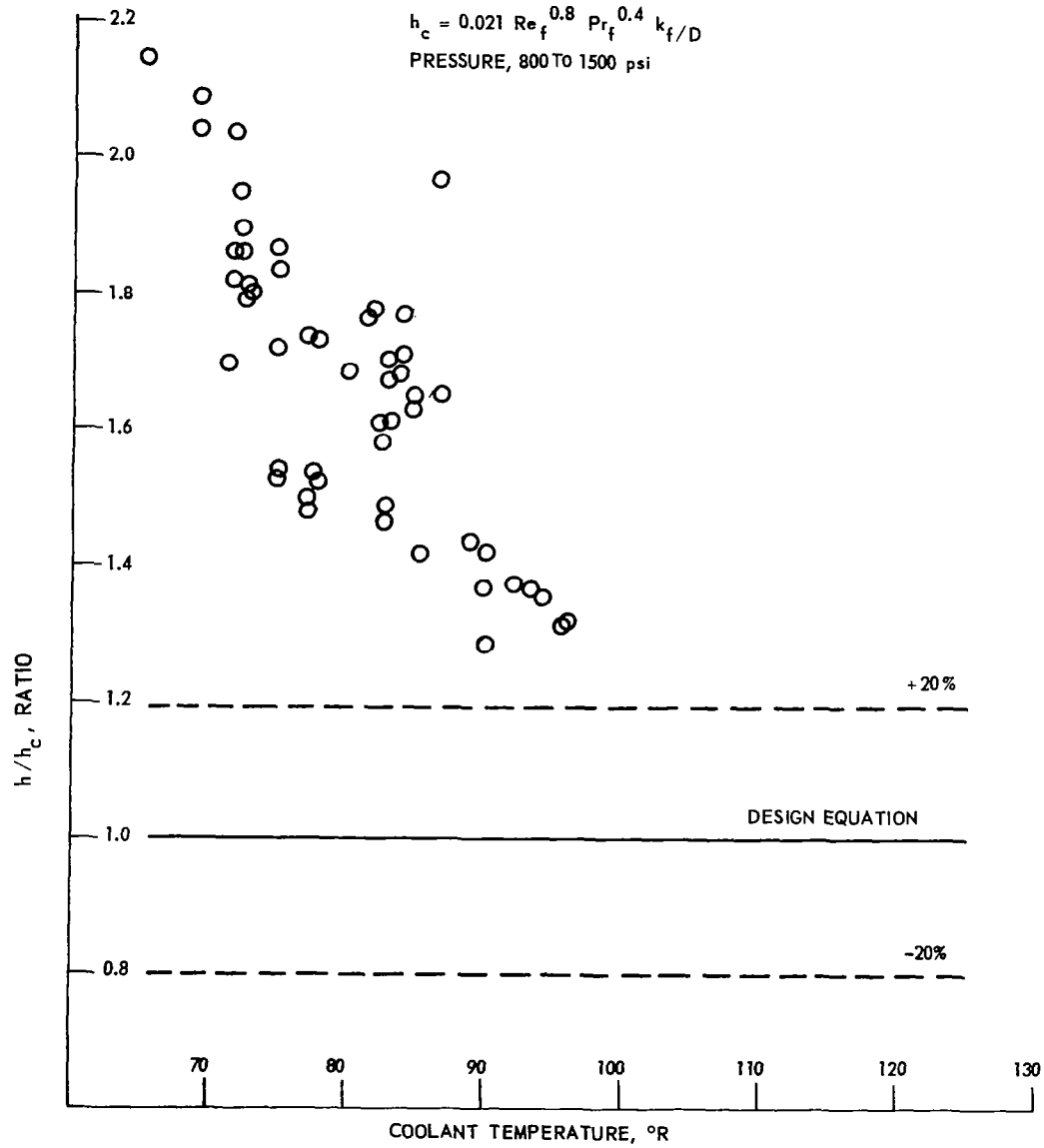

Figure 8

1200 to 1400°R Wall-Temperature Data Compared with Nusselt Equation

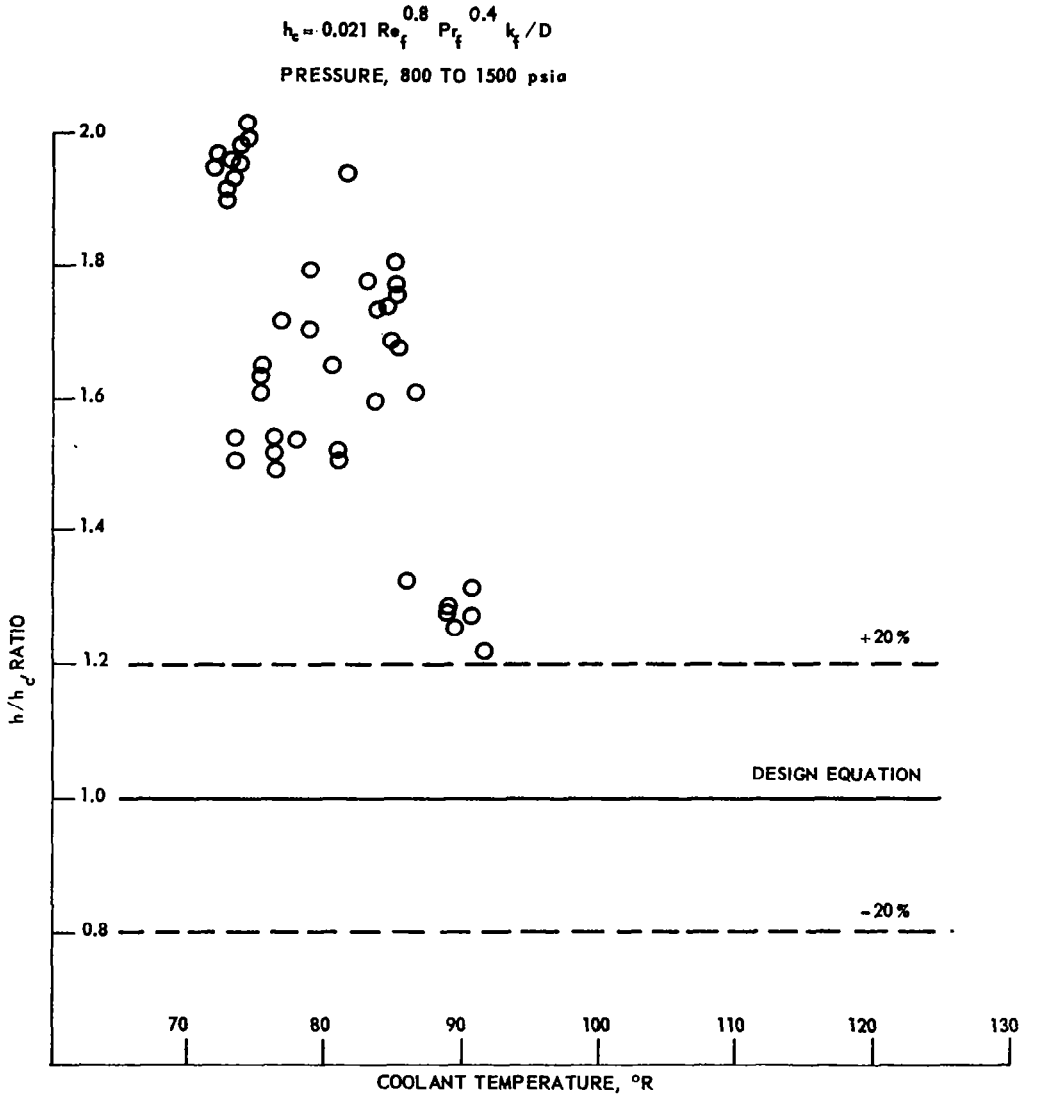

Figure 9

800 to 1000°R Wall-Temperature Data Compared with Hess & Kunz Equation

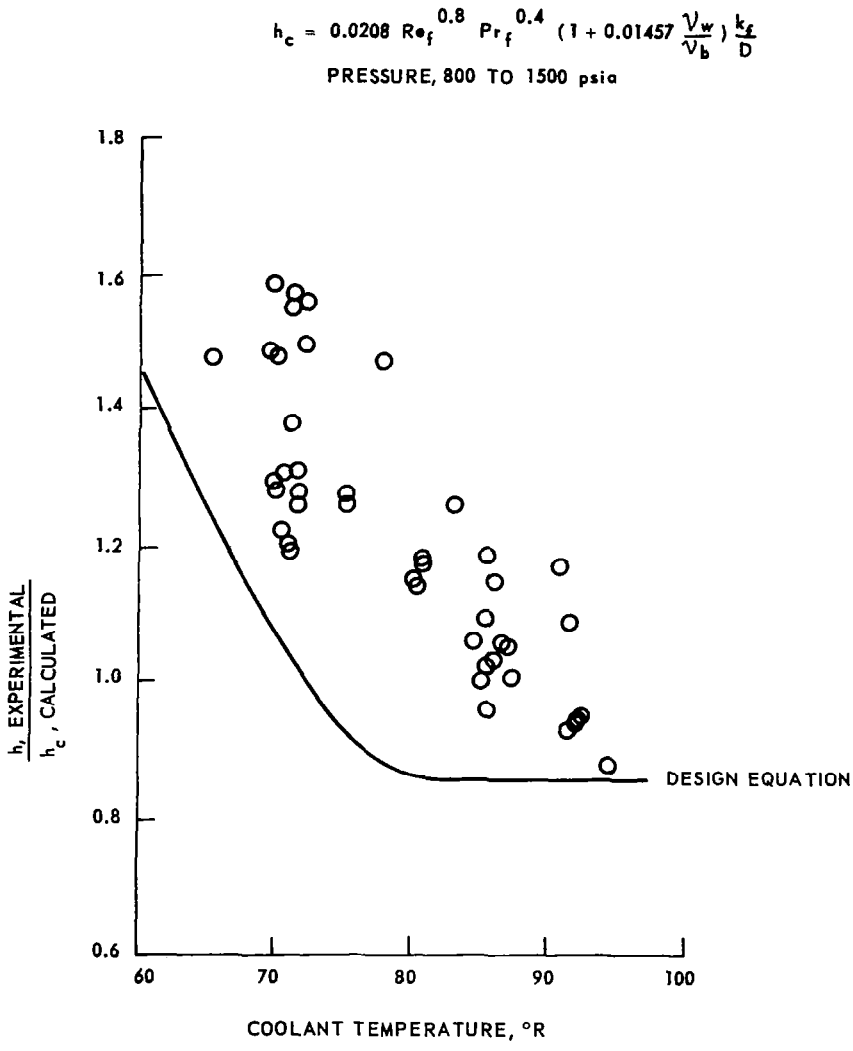

Figure 10

1000 to 1200°R Wall-Temperature Data Compared with Hess & Kunz Equation

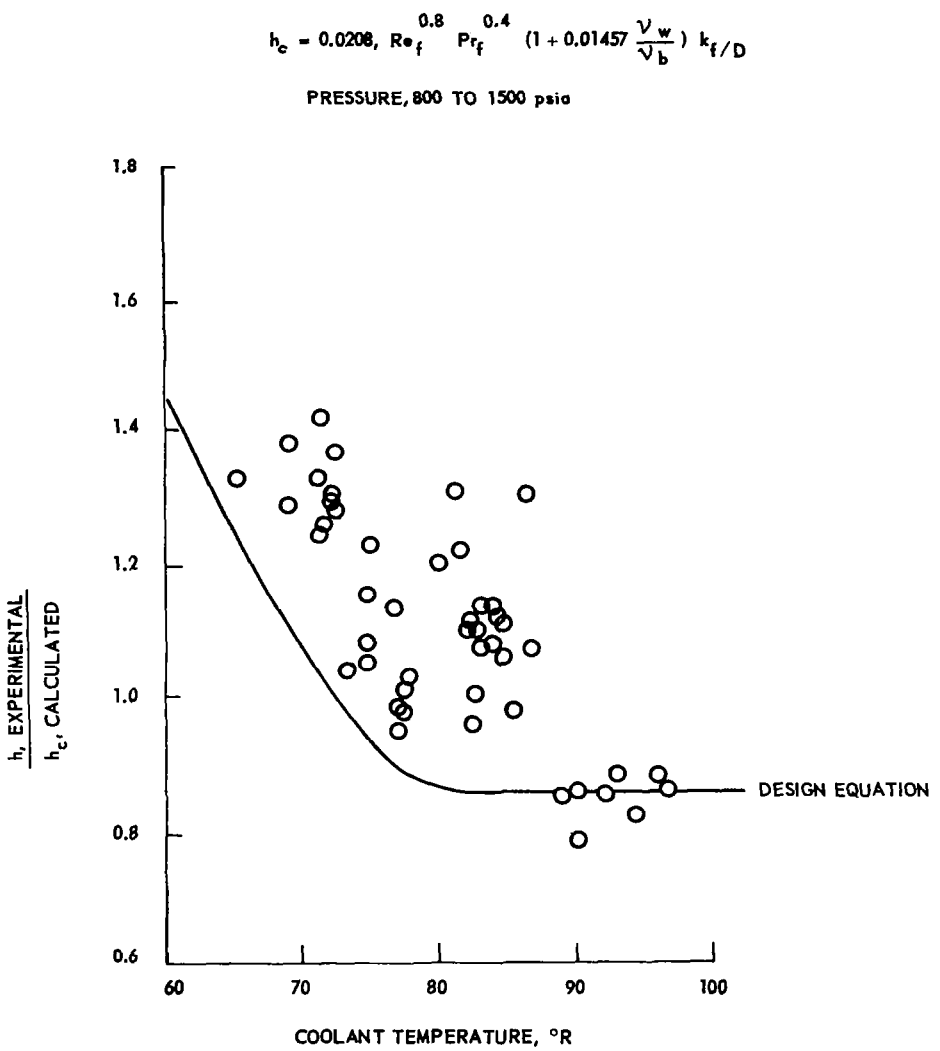

Figure 11

1200 to 1400°R Wall-Temperature Data Compared with Hess & Kunz Equation

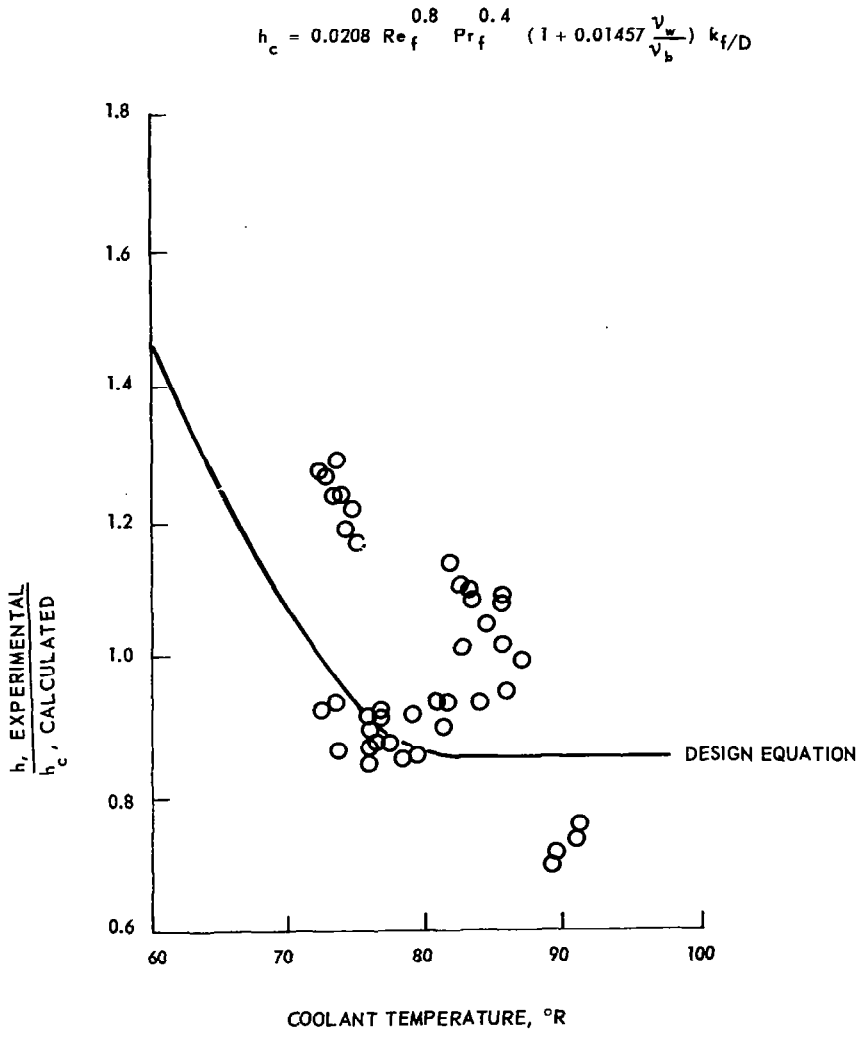

Figure 12

a. Effect of Wall Temperature

The data were segregated on the basis of wall temperature to demonstrate how the inclusion of the term containing the kinematic-viscosity ratio accommodates the different wall temperature regimes. Figure 13 shows all the data from this straight-tube test program compared with the Hess and Kunz equation, and the recommended design equation is indicated. The data are adequately represented by this modified equation.

b. Effect of Heated-Length-to-Diameter Ratio

To achieve the objectives in the straight-tube tests, short test sections were tested, introducing questions regarding entrance or heated-length effects. The test data plotted in Figures 10, 11, and 12 were replotted in Figures 14, 15, and 16 to illustrate possible influence of entrance or heated-length effects. Two effects are evident in these figures: the influence of coolant temperature and the addition to the L/D ratio. The low coolant-temperature effect was accommodated in these figures by using the design equation to compute the predicted heat-transfer coefficient. Any departure from a ratio of 1.0 may now be attributed to other effects, such as entrance effects. A simplified expression for predicting the increase to heat transfer because of a sharp-edge entrance for normal fluids, Reference (10), is also shown in these figures. It is suggested that any entrance or heated-length effect would not exceed the amount predicted by this term. The influence of low coolant temperatures and short heated-length-to-diameter ratios are inter-related; however, it appears that the high experimental coefficient at low coolant temperatures is in addition to any entrance effects and should be handled separately.

2. Curved-Tube Test Data

The experimental test data for the curved-tube test sections were compared with the Hess and Kunz predictive equation in a manner similar to that of the straight-tube data.

Straight-Tube Test Data Compared with Hess & Kunz Equation

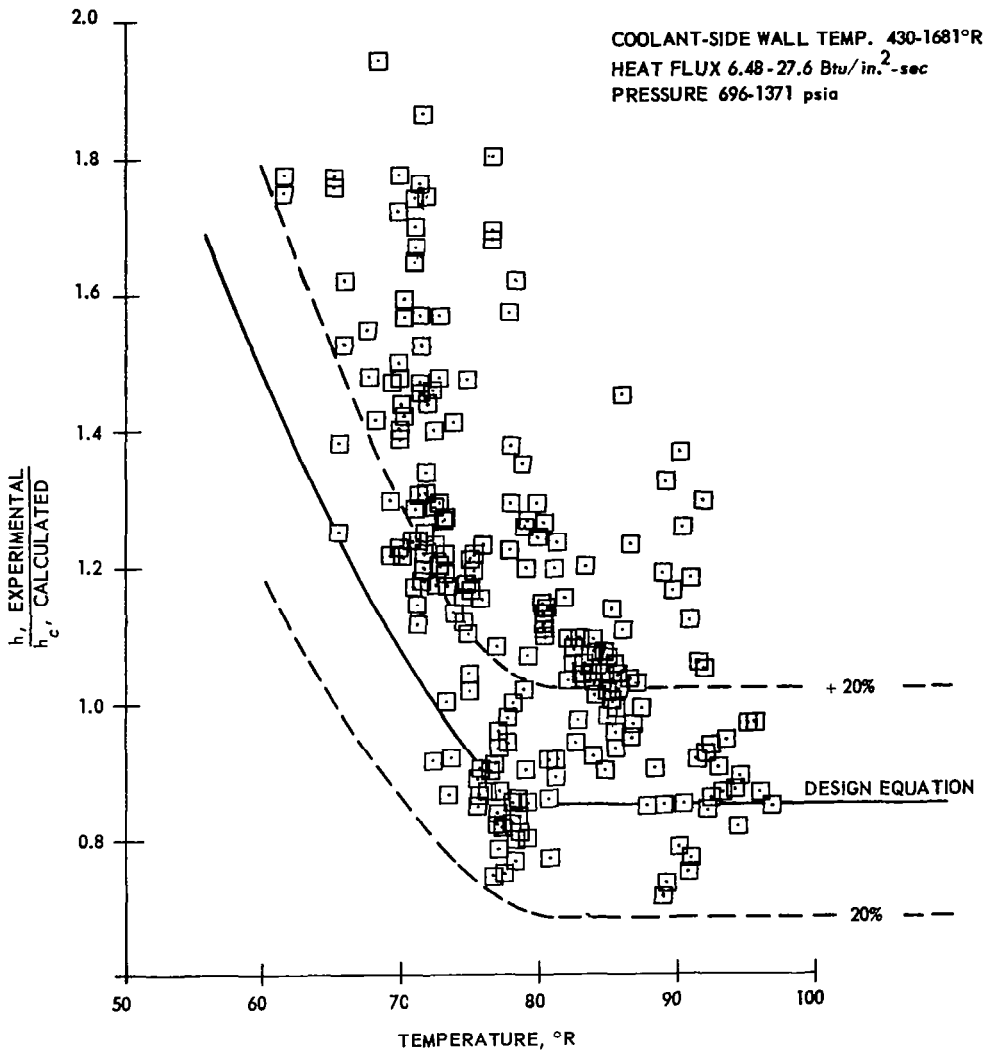

Figure 13

800 to 1000°R Wall-Temperature Data

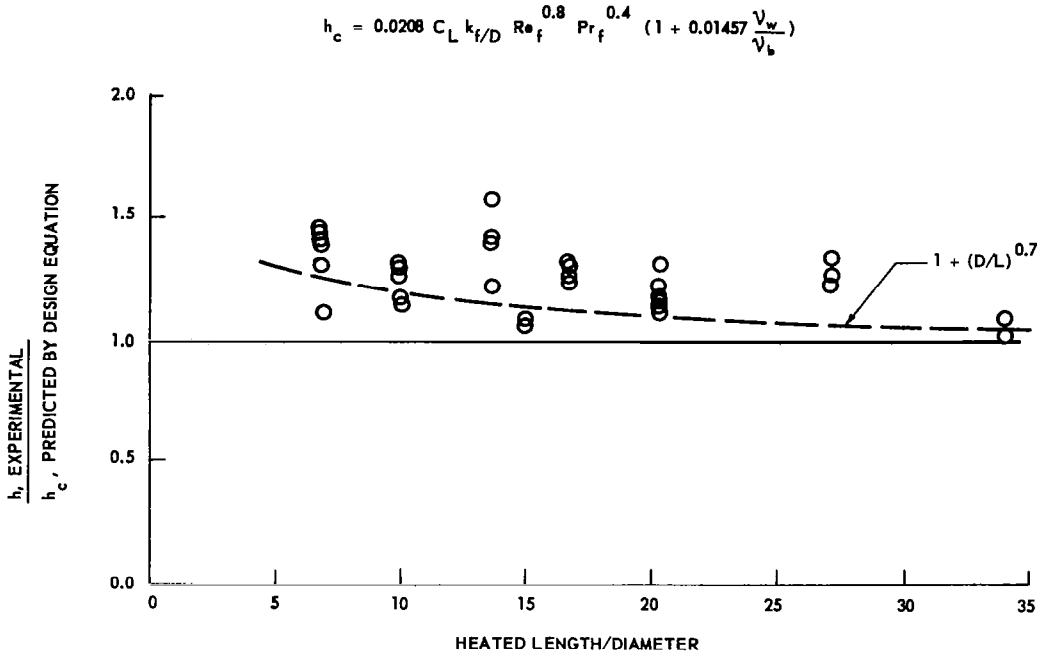

Figure 14

1000 to 1200°R Wall-Temperature Data

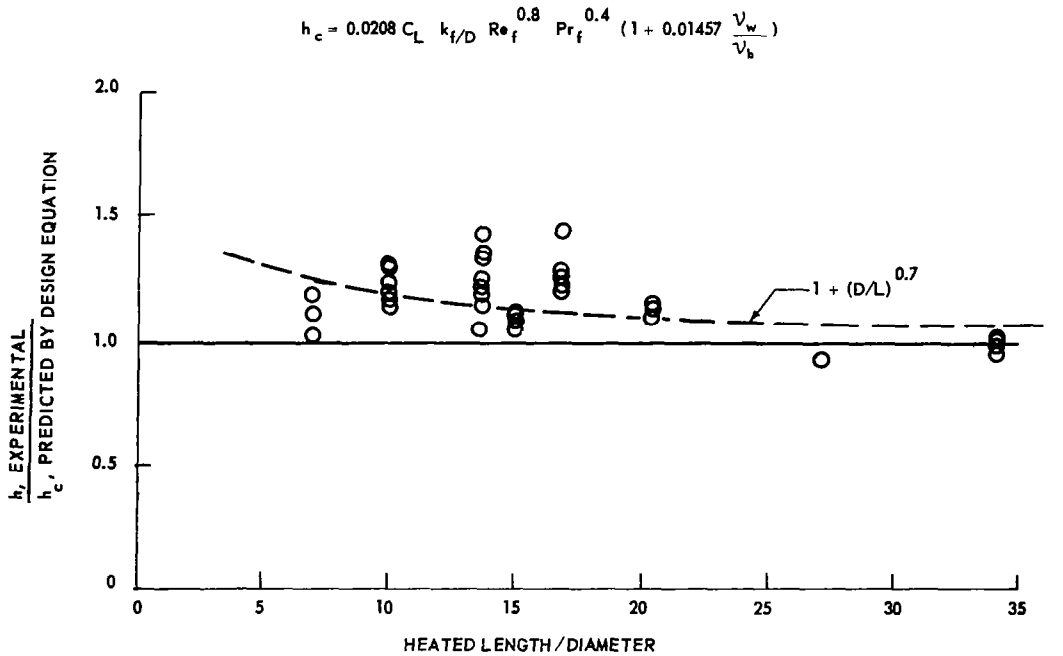

Figure 15

1200 to 1400°R Wall-Temperature Data

$$h_c = 0.0208\, C_L\, k_{f/D}\, Re_f^{0.8}\, Pr_f^{0.4}\, \left(1 + 0.01457\, \frac{\nu_w}{\nu_b}\right)$$

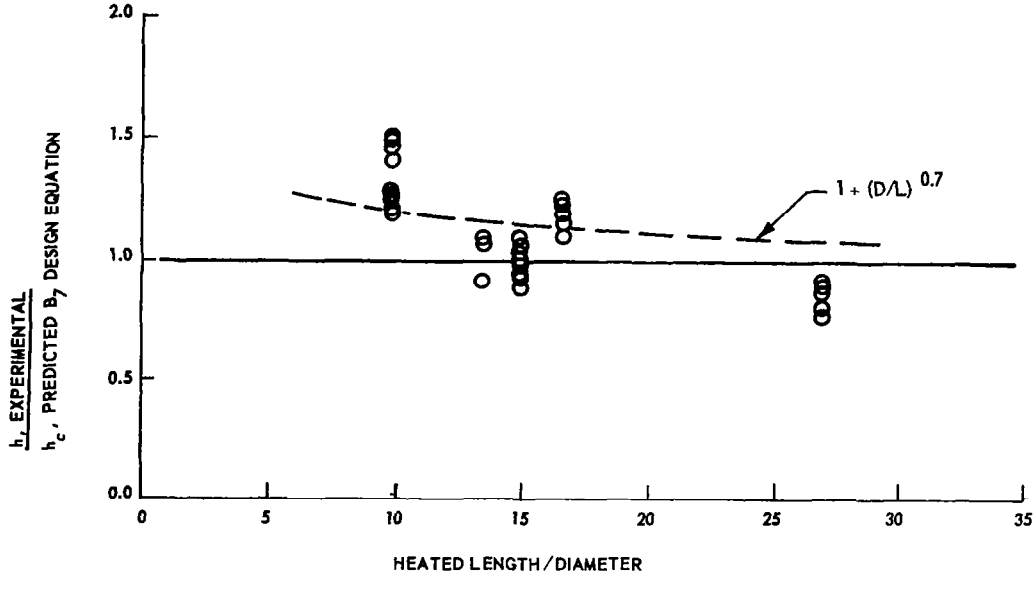

Figure 16

In general, as the coolant moves around the curve the heat-transfer coefficient first increases and then decreases. The significance of this increase in h is evident from an examination of the wall temperature profiles for two of the tests in the non-circular cross-section tubes, shown in Figures 17 and 18.

In Figures 17 and 18 both the experimentally-measured and calculated wall temperatures are plotted, with the calculated wall temperatures based on the Hess and Kunz equation. At the points of tangency on each end of the test section, the experimental and calculated wall temperatures tend to converge, and only diverge significantly near the center of the curve, just as if curvature were effective in increasing h.

The heat-transfer coefficient ratio, h/h_c, was plotted for these same test sections in Figures 19 and 20. These figures illustrate the influence of an increase in the magnitude of the heat-flux parameter, $(Q/A)D^{0.2}/G^{0.8}$, on the prediction of the heat-transfer coefficient. They also illustrate, perhaps more significantly, the influence of tube curvature on the degree of enhancement. For the tube with bend radii of 2 and 4 inches (CAN 2-4, Figure 20) an h/h_c ratio as high as 2:1 was measured, while for the larger bend radii test section (CAN 4-8, Figure 19) the h/h_c ratio was only as high as 1.4:1. In both cases, an increase in the magnitude of the heat-flux parameter resulted in a decrease in the magnitude of the heat-transfer coefficient ratio.

In general, the most severe heat-transfer regime in a rocket nozzle is that region on the URAD side of the geometric throat. In these curved-tube tests this corresponded to an angular position between 17 and 40°. The test data for these two angular positions were plotted in Figures 21 and 22 in the same manner as for the straight-tube data, with the variation in the magnitude of the heat-transfer coefficient ratio plotted as a function of the coolant temperature. The angular positions for these data are nearly the same; however, the L/D ratio varies because of radius of curvature.

For coolant temperatures above 80°R, at the geometric throat (Figure 21) the coefficient for the smaller-bend-radii test sections (closed symbols) range from 1.5 to 2.0 times the calculated, and the coefficient for the larger-bend-radii tubes (open symbols)

Curved-Tube, Wall-Temperature-Profile Test Section CAN 4-8

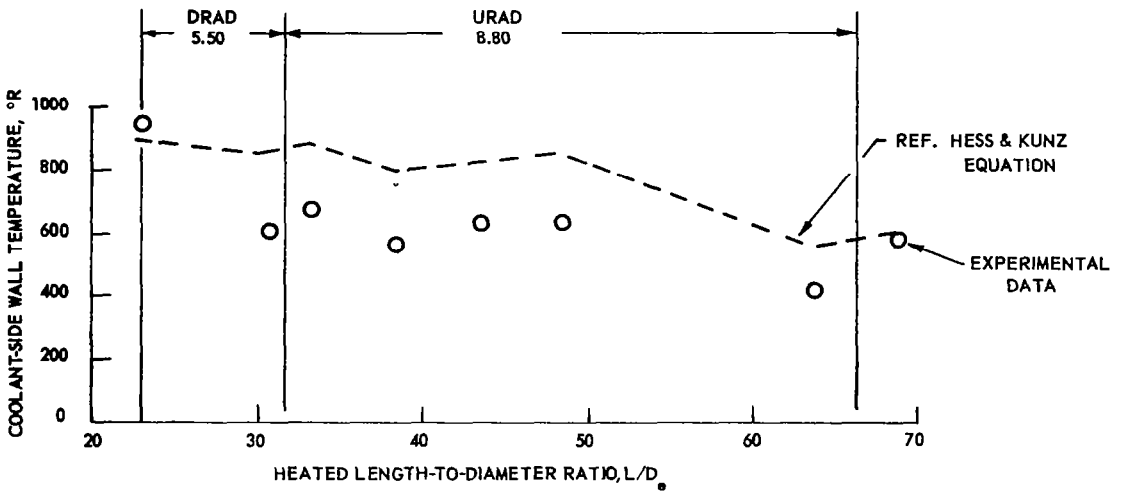

Figure 17

Curved-Tube, Wall-Temperature-Profile Test Section CAN 2-4

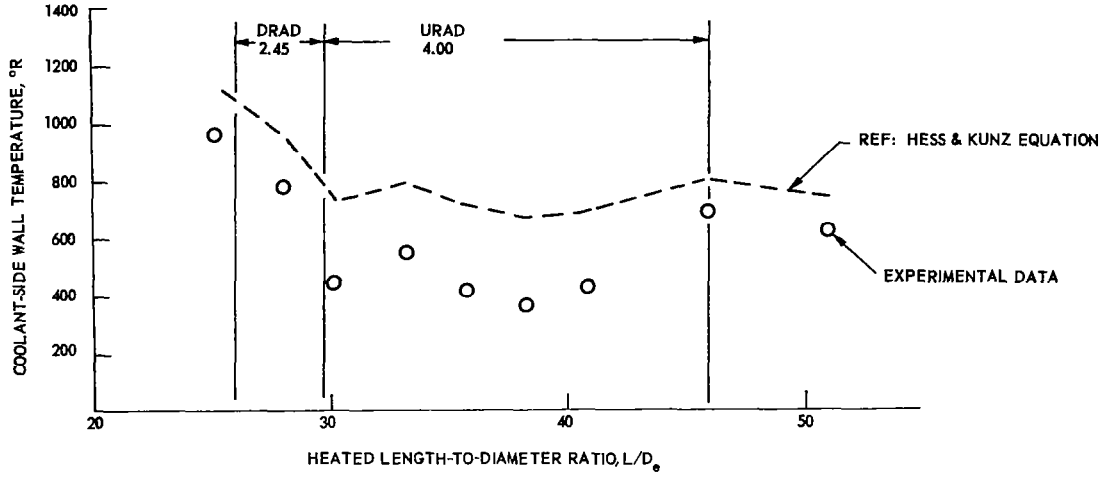

Figure 18

Heat-Transfer-Coefficient Ratio,
Curved-Tube Test Section CAN 4-8

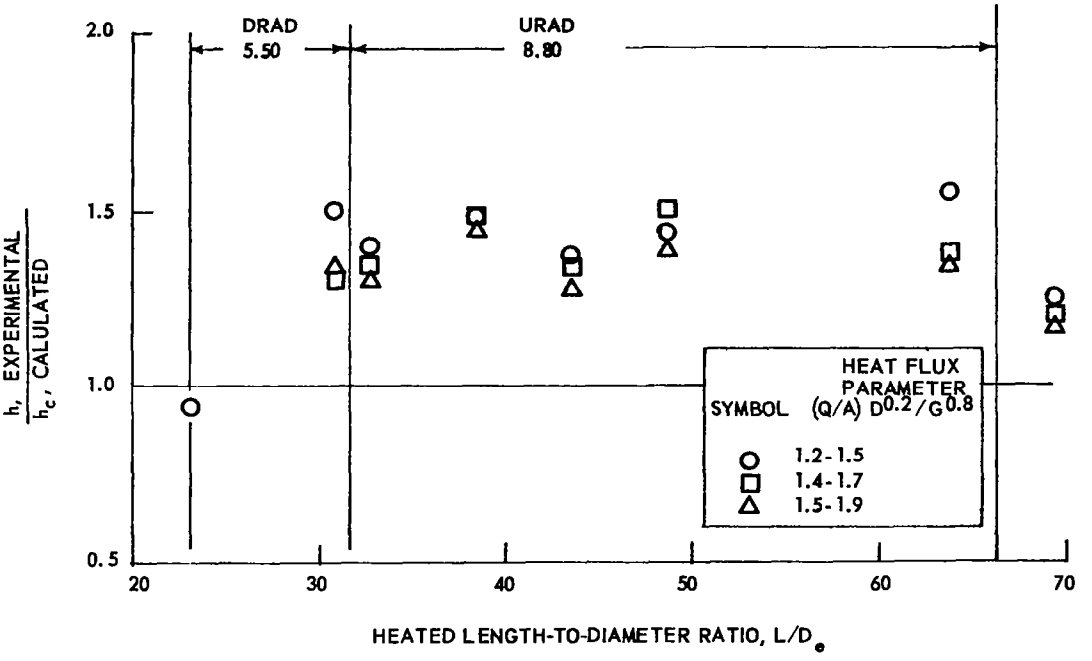

Figure 19

Heat-Transfer-Coefficient Ratio,
Curved-Tube Test Section CAN 2-4

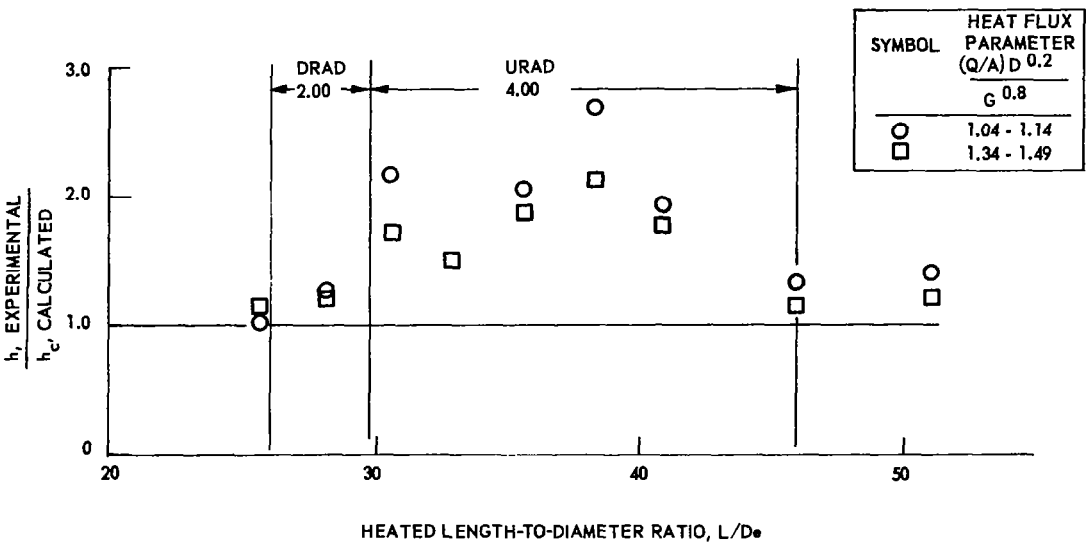

Figure 20

Curved-Tube Test Data for Simulated Throat Region

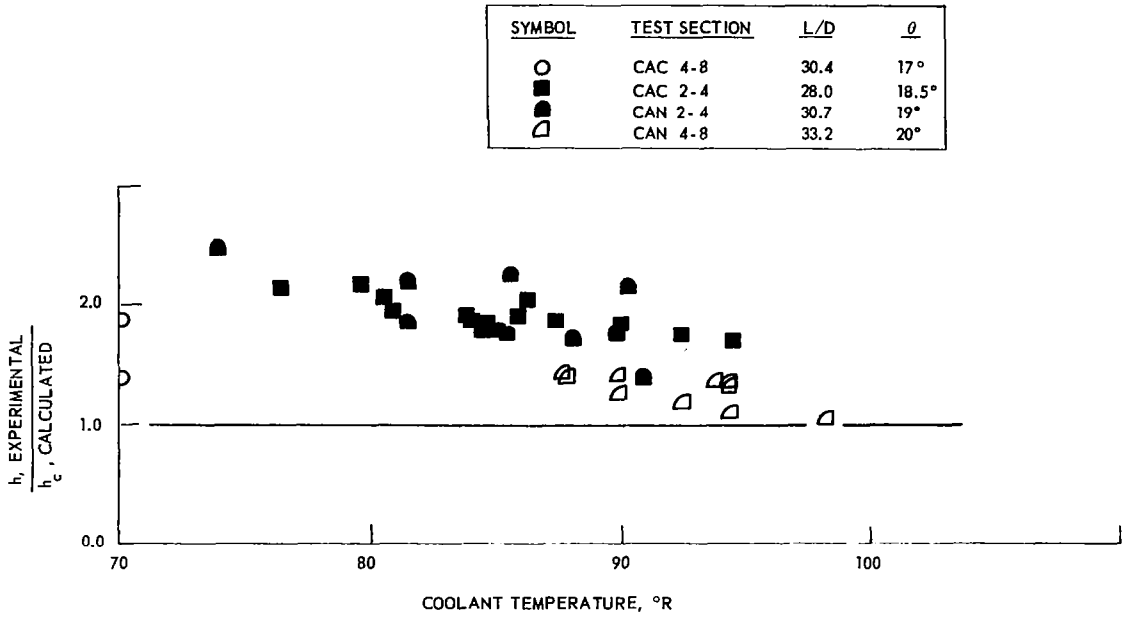

Figure 21

Curved-Tube Test Data for Simulated Maximum-Flux Region

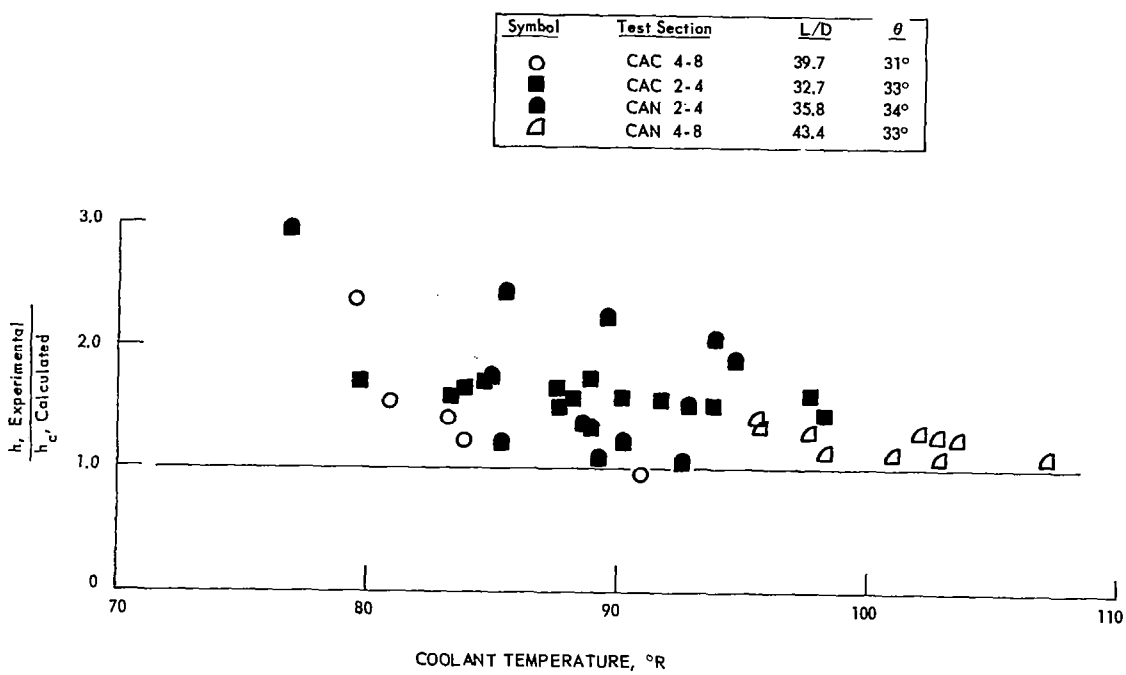

Figure 22

range from 1.0 to 1.4 times the calculated, based on the Hess and Kunz equation. These data exceed the prediction based on Equation (3) for curved tubes. With developed distance around the curve the enhancement decreases (Figure 22); however, the coefficient remains as high as or higher than that predicted by Equation (3) for curved tube.

C. PRESSURE DROP

1. Straight Tube

Considerable variation was noted in the pressure drop data. In general, the frictional pressure drop was less than 30% of the measured static pressure drop; consequently, the influence of the pressure drop caused by the increase in velocity tended to obscure the frictional pressure drop. Data from tests in the straight 6-in. test section without heat addition and the 3-in. high-heat-flux test section with heat addition are presented in this analysis. The computed coefficient of friction, $f/2$, is plotted in Figure 23 as a function of Reynolds' number. The simplified equation used to predict the friction factor is also shown, indicating the degree of conformance between the predicted and the experimental. The data are somewhat inconclusive; however, it seems that the prediction of the heat-transfer coefficient by this method is not completely invalid since it represents about 50% of the data. The straight-tube pressure-drop data are shown in Table 5.

2. Curved Tube

The proper treatment of the pressure drop in a curved pipe realistically calls for a measure of the static pressure at the points of tangency on the curve. The location of the pressure taps as near the inlet and outlet electrodes (outside the heated length) as possible was therefore a compromise which increased the difficulty in interpretation of the test results, but simplified the experimental system. It was intended that the magnitude of the enhancement in the heat transfer coefficient be compared with the pressure loss predicted by a simple parameter involving various radii and Reynolds numbers. Demonstration that the parameter proposed by Ito represents the measured enhancement in heat transfer would then be evidence that Reynolds' analogy holds and

Variation of Experimental Friction Factor with Bulk Reynolds Number

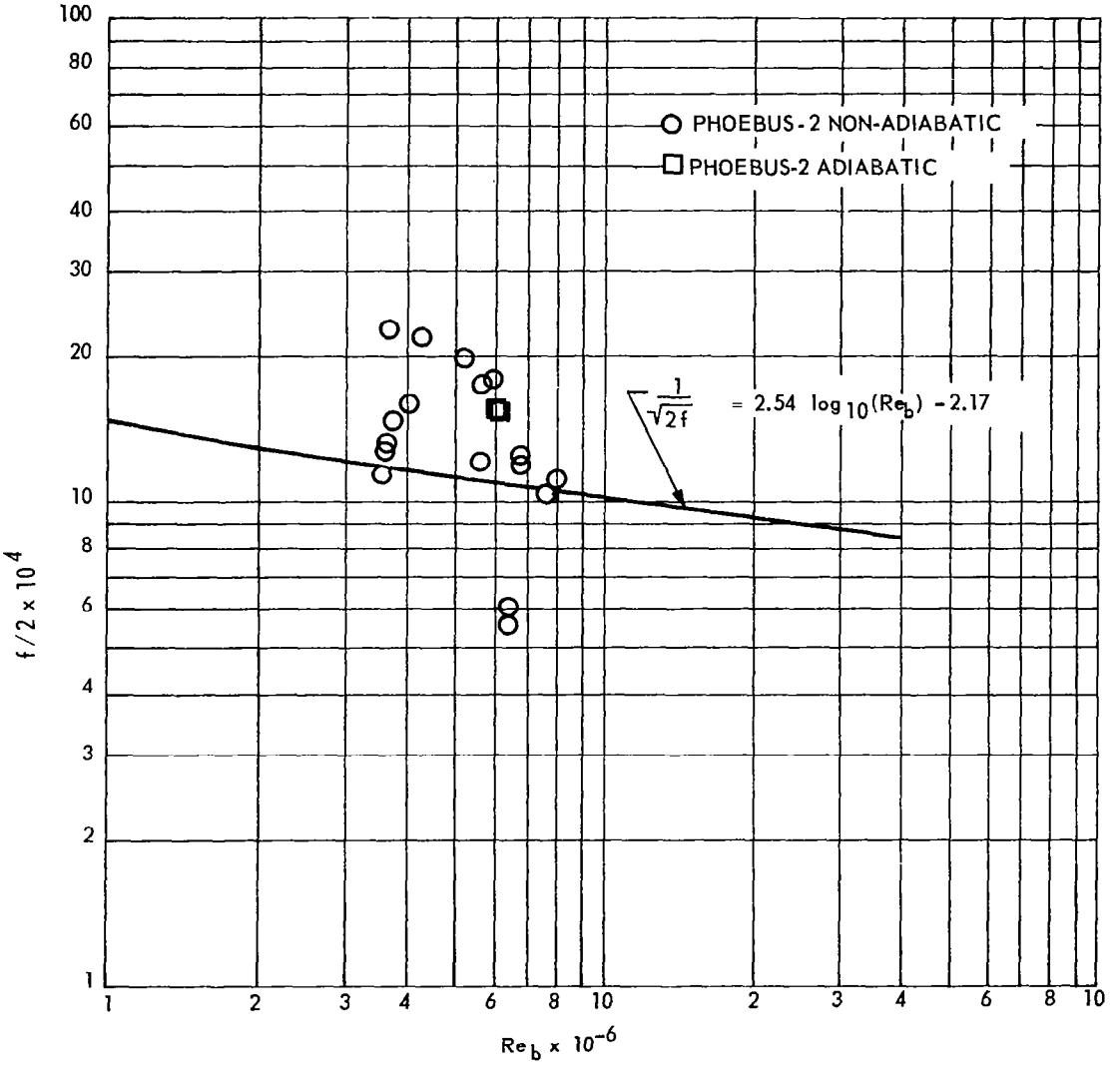

Figure 23

TABLE 5

PRESSURE DROP IN STRAIGHT TUBES

T_1 (°R)	P_1 (psia)	T_2 (°R)	P_2 (psia)	ΔP (psi)	ΔP_v (psi)	ΔP_f (psi)	f/2 ---	Re_b X10^{-6}
61.6	880.1	68.3	851.0	28.9	17.28	11.62	0.0023	3.77
64.2	1176.0	69.9	1138.0	38.0	20.05	17.95	0.0022	4.38
70.3	1273.0	81.1	1245.0	28.0	22.46	5.54	0.0012	3.67
71.5	1256.0	83.0	1228.0	28.0	23.32	4.68	0.0011	3.63
65.2	912.1	71.7	846.6	65.5	45.54	19.96	0.0018	6.03
70.0	1081.0	80.6	1053.0	28.0	21.89	6.11	0.0014	3.76
66.0	877.3	73.3	824.7	52.6	36.99	15.61	0.0019	5.32
69.2	938.9	79.1	906.4	32.5	25.98	6.52	0.0016	4.11
65.6	754.0	72.4	695.5	58.5	42.22	13.28	0.0017	5.67
71.5	1213.0	82.5	1186.0	27.0	21.90	5.10	0.0013	3.67
72.4	1186.0	83.9	1159.0	27.0	22.10	4.90	0.0013	3.66
71.2	1144.0	80.2	1087.0	57.0	45.70	11.30	0.0012	5.71
70.0	971.9	77.0	896.0	75.9	61.40	14.50	0.0012	6.85
71.0	953.7	78.1	878.9	74.8	60.80	14.00	0.0012	6.88
68.4	1013.0	74.9	915.7	97.3	79.20	18.10	0.0010	7.70
70.6	1118.0	78.0	1012.0	106.0	85.30	20.70	0.0011	8.08
71.6	1289.0	81.5	1212.0	77.0	68.90	8.10	0.0006	6.46
71.9	1259.0	81.9	1184.0	75.0	68.00	6.90	0.0005	6.45
76.7	1097.0	83.4	967.5	129.5	115.10	14.40	0.0010	9.70
56.6	1299.0	57.5	1088.0	211.0	25.50	185.50	0.00156	6.16
57.4	1262.0	58.8	1055.0	207.0	25.40	181.60	0.00155	6.29
56.6	1299.3	58.0	1086.6	212.7	29.10	183.60	0.00154	6.21

the enhancement can be predicted. The relationship developed by Ito (Equation 3) was evaluated for the non-circular cross-section flow area tubes for comparison with the test data. The radius of the tubes was defined as $D_e/2$. The Reynolds number used was an arithmetic average between the inlet and the outlet. The overall coefficients of friction for the curved non-circular cross-section are shown in Table 6, and are also plotted in Figure 24. If one compares the magnitude of the coefficient of friction for these two test sections with the prediction equation it is apparent that the measured increase in the heat-transfer coefficient corresponds to the apparently high-friction coefficient for the curved tubes.

The estimate of the magnitude of the increase in resistance around the curve based on Equation (3) for the two test-section geometries is indicated as a dashed line in Figure 24. The experimental results for the CAN 2-4 section are considerably higher than predicted by Ito's equation.

D. SYSTEM OR TEST-SECTION OSCILLATIONS

Hendricks, Reference (1), reported high-frequency oscillations in some tests conducted in straight tubes. System vibration was apparently present in all tests at a frequency at or below 1000 cps, which did not influence heat transfer; however, in certain tests, high-frequency oscillations were observed and a variation in the heat-transfer coefficient was noted. Since it is possible that vibration may be present and that the heat-transfer results may have been significantly affected, the first curved-tube test was conducted with accelerometers mounted on the electrodes to detect vibrations parallel to the coolant-flow channel and transverse to the axis of the coolant tube (as shown on Figure 25). The test section was restrained in the axial direction by the flow system and, except for the flexible bus bar connections, was not constrained in the transverse direction.

Two Endevco Model 2214 accelerometers, with a flat frequency response to 9000 cps, were mounted on the inlet test-section electrode. The output of the accelerometers was fed to high-response galvanometers and recorded on an oscillograph recorder with a paper speed of 115 in./sec. On this test two zero power and twelve steady state

TABLE 6

PRESSURE DROP IN CURVED TUBES

Test Section CAN 2-4

T_1 (°R)	P_1 (psia)	T_2 (°R)	P_2 (psia)	ΔP (psi)	ΔP_v (psi)	ΔP_f (psi)	f/2 --	Re_b $x10^{-6}$
54.2	1230	100.4	1168.0	62.0	24.3	37.7	.00245	4.04
55.0	1222	113.5	1162.0	60.0	25.8	34.2	.00210	4.16
54.6	1034	99.7	912.6	121.4	53.7	67.7	.00198	5.96
60.8	1225	102.7	1081.0	144.0	60.0	84.0	.00219	6.66
61.0	1226	103.1	1083.0	143.0	59.9	83.1	.00217	6.66
54.9	1241	111.0	1180.0	61.0	23.4	37.6	.00254	3.95

Test Section CAN 4-8

T_1 (°R)	P_1 (psia)	T_2 (°R)	P_2 (psia)	ΔP (psi)	ΔP_v (psi)	ΔP_f (psi)	f/2 --	Re_b $x10^{-6}$
59.2	1259	116.5	1208	51	20.2	30.8	.0017	3.47
60.5	1200	119.4	1140	60	24.2	35.8	.0017	3.83
63.3	1155	125.9	1090	65	27.2	37.8	.0016	4.14
63.7	1153	127.0	1088	65	27.2	37.8	.0016	4.14
57.8	1251	116.8	1188	63	26.0	37.0	.0016	3.85
58.9	1241	130.0	1178	63	25.3	37.7	.0017	3.91

Curved-Tube Friction Factor

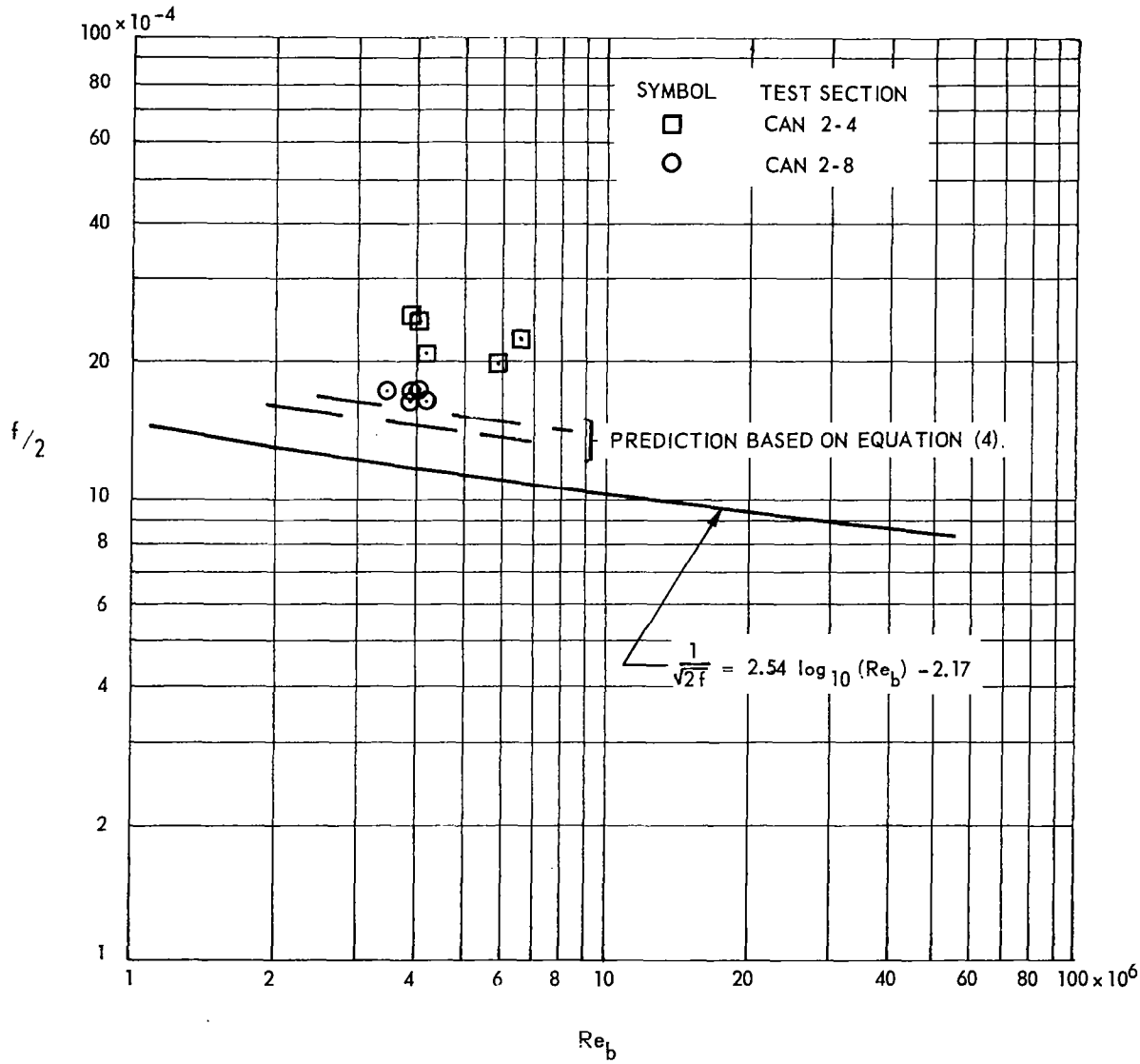

Figure 24

Accelerometer Installation

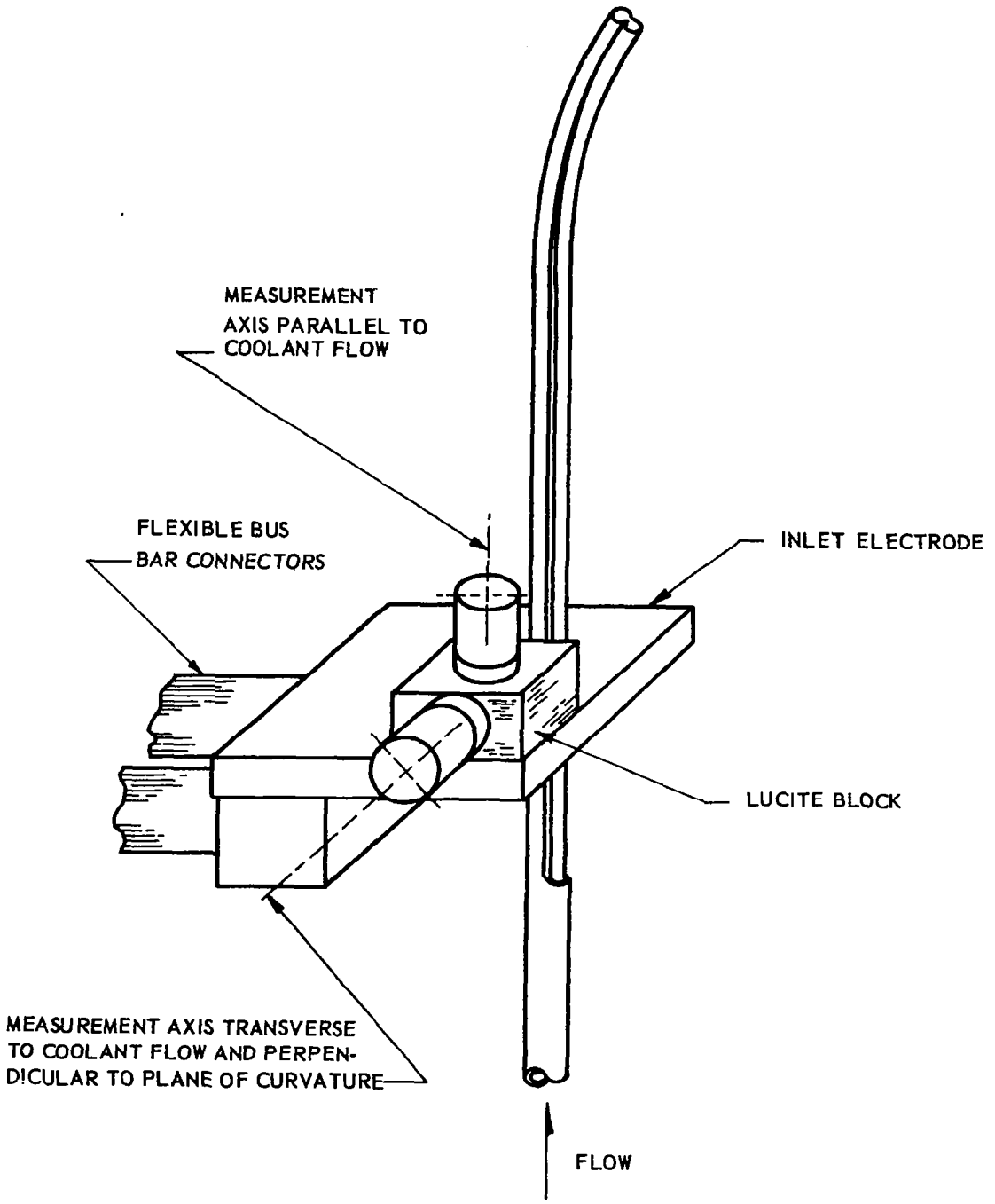

Figure 25

points with various power inputs in the test section were recorded. Results of the measurements are shown in Table 7, along with the fluid-flow rate and power input to the test section. The measurements indicated that the system vibrated along both axes with the amplitude and frequency along the longitudinal axis being lower than in the transverse direction. The transverse frequencies were varied and appeared to exceed 9000 cps at amplitudes to 2 g's. The frequency seemed to be influenced by the weight-flow-rate rather than the application of power. In general, an increase in flow rate was accompanied by an increase in the amplitude of the oscillations, regardless of the power. This is illustrated by Figure 26, a plot of the measured accelerations as a function of weight-flow-rate.

The test results were inconclusive with respect to system vibration affecting heat transfer. In Reference (1), the tests in which the heat transfer process was affected, a lateral oscillation was heat driven and decayed when power was removed. In these tests there was no apparent change in frequency, either with or without power. This test was not adequate to determine whether or not the heat transfer was affected.

VI. CONCLUSIONS AND RECOMMENDATIONS

The experimental test data from the straight and the curved-tube tests were compared with the Hess and Kunz film temperature equation. It was concluded that this equation can be suitably modified to represent the test data for design and predictive purposes.

A. STRAIGHT TUBE TESTS

The straight-tube test data were compared with Equation (3) which had been devised to empirically represent the available liquid-side test data. In this design equation a variable coefficient, C_L, was included to account for a departure of the data from the values predicted for low coolant temperatures. The test data compared with this equation covered heat fluxes from 6.4 to 27.6 Btu/in.^{2}-sec and coolant-side wall temperatures from 430 to 1680°R. Achievement of the desired test conditions of high-heat fluxes at coolant temperatures between 80 and 100°R resulted in the use of short test sections. Consequently, a question is raised as to the possible influence entrance effect or short

TABLE 7

SUMMARY OF VIBRATION TEST RESULTS HT-3-116

February 18, 1966

Data Point	Longitudinal Axis		Transverse Axis		Power Input (Btu/sec)	Weight, Flow Rate (lb/sec)
	Freq (cps)	Ampl (g's)	Freq (cps)	Ampl (g's)		
A-1	3-5000	0.5	9000	1.6	0.0	.533
B-1	4000	0.2	9-10,000	0.5	0.0	.338
B-2	4000	0.6	9000	1.2	53.6	.457
B-3	4500	0.6	9-10,000	1.2	63.8	.395
C-1	4000	0.4	9000	0.6	48.9	.296
C-2	4000	0.4	9000	1.4	65.2	.368
C-3	4000	0.4	8-9000	1.2	70.2	.320
D-1	4000	0.4	9000	1.5	36.3	.405
D-2	4000	0.6	9000	1.6	36.3	.454
E-1	4500	0.2	9000	0.4	50.7	.297
E-2	4-4500	0.4	9000	1.2	60.1	.370
E-3	4000	0.8	7-9000	1.6	59.5	.510
E-4	4000	1.1	9000	1.4	55.5	.510
E-5	4-4500	1.2	9-10,000	2.0	52.1	.500

Variation of Acceleration with Weight-Flow-Rate
Test HT-3-116, 18 February 1966

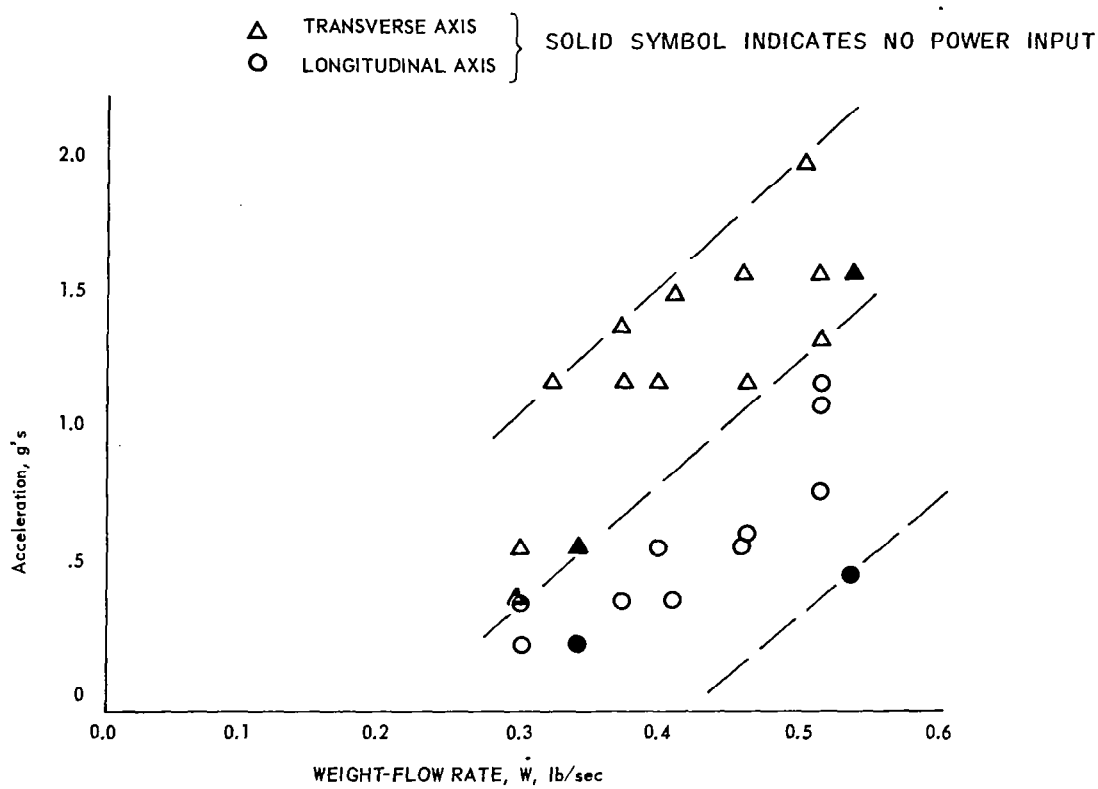

Figure 26

L/D's might have on the heat-transfer coefficient. The heated length-to-diameter ratio is not insignificant with normal fluids in turbulent flow, therefore the test data were compared in terms of the heated length-to-diameter ratio. It appeared from this examination that an L/D effect could be considered separate from the bulk temperature effect. It is therefore contended that the increase in the predicted heat-transfer coefficient at low coolant temperature is to account for an inadequacy of the equation and not to account for some undefined entrance effect. Subsequent to the completion of the straight-tube tests, Reference (1) noted unusual test results in which an abnormally high heat-transfer coefficient was measured in certain test results. The only significant difference between the tests with high heat transfer and others was the presence of high-frequency oscillation of the test section. Vibration measurements were not made on the straight-tube test sections, and it is not known if vibrations were present or, if present, whether or not they modified the test results by either enhancing or degrading the rate of heat transfer. High heat fluxes with Hastelloy X tubing were achieved when several tests were performed with heat fluxes in excess of 20 Btu/in.^{2}-sec. The pressure drop data from these tests varied significantly, which makes interpretation awkward; however, it seems that the method presently used is adequate.

B. CURVED-TUBE TESTS

The curved-tube tests were conducted in asymmetrically-heated test sections of two geometries, the Phoebus-2 design curvature with a DRAD-URAD of 4.00 and 8.00 inches, respectively, and an off-design contour with a DRAD-URAD of 2.00 and 4.00 inches. Both circular and flattened (or non-circular) cross-sectional flow area tubes were tested.

Perturbations in the analysis of the results attendant with short L/D's, or entrance effects, and low coolant temperatures were avoided in the curved-tube tests by employing a straight section upstream of the first thermocouple station in excess of 20 diameters. This straight section served to establish a thermal boundary layer and also preheat or condition the fluid to a coolant temperature

of approximately 80°R, or higher, before the coolant reached the curved portion of the test section. Any measured enhancement should be relatively unaffected by L/D and/or low-coolant-temperature effects attendant with the straight-tube tests. Comparison of these test data with the Hess and Kunz equation indicated that:

1. The heat-transfer coefficient on the concave (or outside of the curve) was enhanced by a factor as high as 2:1.

2. An increase in the radii of curvature decreases the magnitude of the enhancement.

3. There was no significant adverse effect caused by either asymmetric heating or non-circular flow areas.

4. From the standpoint of design, it seems that the smaller DRAD results in a much faster increase in the heat-transfer enhancement. Development of maximum enhancement occurs in a shorter developed length for a DRAD of 2.0 in. and persists further than for the DRAD of 4.0 in.

5. For the Pheobus-2 contour the degree of enhancement at the point corresponding to critical, or high heat flux, region in the nozzle varies by a factor of 1.0 to 1.4 times that predicted by the Hess and Kunz equation.

A comparison of the calculated average friction factors tends to substantiate the heat-transfer results. The friction factor was higher for the tests with higher heat-transfer coefficients. The increase in resistance to flow around a curve was supported by the results of the non-circular flow area Phoebus-2 contour tube; however, the heat-transfer coefficient and the pressure drop were both understated by the Ito relationship for the off-design contour. Vibration was measured at the inlet electrode of the test section, however, it could not be definitely established that the vibration was or was not affecting the heat-transfer results.

REFERENCES

1. R. C. Hendricks, R. J. Simoneau, and R. Friedman, Heat-Transfer Characteristics of Cryogenic Hydrogen from 1000 to 2500 psia Flowing Upward in Uniformly Heated Straight Tubes, NASA Technical Note TN-D-2977, September 1965

2. W. S. Miller, J. D. Seader, and D. M. Trebes, Forced Convection Heat Transfer to Liquid Hydrogen at Supercritical Pressures, presented at the International Institute of Refrigeration, Commission I, Grenoble, France, 9-11 June 1965.

3. W. S. Miller, J. D. Seader, and D. M. Trebes, Supercritical Pressures Liquid Hydrogen Heat Transfer Data Compilation, Rocketdyne Report R-6129, 21 April 1965.

4. H. L. Hess and H. R. Kunz, "A Study of Forced Convection Heat Transfer to Supercritical Hydrogen", Trans., ASME, Journal of Heat Transfer, Series C, 1965, pp. 41-48.

5. E. L. Geery and W. R. Thompson, Design Equation Analysis for Heat Transfer to Cryogenic Hydrogen at Pressures from 600 to 1500 psia and Wall-to-Bulk Temperature Ratios to 20, Aerojet-General REON Report RN-S-0274, April 1966.

6. R. C. Hendricks and F. F. Simon, "Heat Transfer to Hydrogen at Near Critical Temperatures and Supercritical Pressures Flowing in a Curved Tube", Proceedings, Multi-Phase Flow Symposium, H. J. Lipstein, ed., ASME, 1963, p. 90.

7. An Experimental Investigation of Heat Transfer to Hydrogen at Near Critical Temperatures and Supercritical Pressures Flowing Turbulently in Straight and Curved Tubes, Aerojet-General, Azusa, REON, Report 2551, May 1963.

8. H. Ito, "Friction Factors for Turbulent Flow in Curved Pipes", Basic Engineering, Trans. ASME, Series D, Vol. 81, 1959, p. 123.

9. O. A. Farmer, Para-Hydrogen Properties Code (TAB), Transmitted by Los Alamos Scientific Laboratory Memorandum No. N-4-2324 to SNPO-C, 28 September 1964.

NOMENCLATURE

A	Asymmetrically heated tube
C	Curved tube, circular cross-section
C_L	Variable coefficient in modified Hess & Kunz equation
C_p	Specific heat at constant pressure, Btu/lbm^{o}R
D	Inside diameter of tube, in.
De	Equivalent diameter of tube, in.
f	Friction factor
f_c/f_s	Ratio of resistance to flow in curved and straight tube
g_c	Conversion coefficient, in.-lbm/lbf-sec^2
G	Mass velocity, lb/in.^{2}-sec
h	Heat transfer coefficient, Btu/in.^{2}-sec^{o}R
h_c	Calculated heat transfer coefficient
k	Thermal conductivity, Btu/in.-sec-^{o}R
L	Heated length of tube, in.
Nu	Nusselt number, h D/k
P	Pressure, lbf/in.^{2} (psia)
Pr	Prandtl Number, $C_p \mu / k$
Q_p	Electrical energy input, Btu/sec
Q_R	Sensible energy removed by test fluid, Btu/sec
Q_L	Energy lost through conduction, radiation, and convection, Btu/sec
Q/A	Heat flux, Btu/in.^{2}-sec.
r	Radius of tube, in.
R	Radius of curvature
Re	Reynolds number, D G/μ
T	Temperature, ^{o}R
V	Velocity, ft/sec
ρ	Density, lbm/in.^{3}
μ	Viscosity, lbm/in. sec
υ	Kinematic Viscosity μ / ρ, in.^{2}-sec

SUBSCRIPTS

b	Properties evaluated at the average coolant temperature, T_b
f	Properties evaluated at film temperature, $T_f = 0.5\ (T_b + T_w)$
i	Calculated inner wall temperature
w	Measured outer wall temperature, or properties evaluated at wall temperature, T_w

APPENDIX A

STRAIGHT TUBE TEST DATA

Appendix A

TEST: D123LC-1

Data Point	Station	Pressure P_b (psi)	Temperature Bulk T_b (°R)	Temperature Wall T_i (°R)	Unit Heat Flux Q/A (Btu/in.^{2}-sec)	Heat Transfer Coefficient h (Btu/in.^{2}-sec-°R)	Velocity V (ft/sec)
2	3	990	71.2	776	7.37	.01047	266
	4	990	71.2	740	7.39	.01104	266
3	3	970	75.7	1363	9.66	.007501	301
	4	970	75.7	1321	9.66	.007757	301
4	3	971	75.6	1372	9.52	.00734	299
	4	971	75.6	1328	9.53	.00761	299
5	3	1041	77.1	1124	8.36	.007984	290
	4	1041	77.1	1096	8.37	.008213	290
6	3	901	70.8	913	8.06	.00957	286
	4	901	70.8	859	8.09	.01027	286
7	3	902	71.3	965	8.06	.00903	286
	4	902	71.3	941	8.08	.00928	286
8	3	894	77.1	1468	9.93	.00714	319
	4	894	77.1	1358	9.93	.00775	319
9	3	891	79.2	1440	10.14	.00744	330
	4	891	79.2	1373	10.14	.00783	330
10	3	1086	74.9	1058	8.67	.00882	288
	4	1086	74.9	1032	8.68	.00907	288
11	3	1080	78.5	1470	10.24	.00736	302
	4	1080	78.5	1418	10.23	.00764	302
12	3	1081	78.4	1480	10.18	.007257	303
	4	1081	78.4	1422	10.17	.007567	303

Appendix A

TEST: D123LC-1

Data Point	Station	Pressure P_b (psi)	Temperature Bulk T_b (°R)	Temperature Wall T_1 (°R)	Unit Heat Flux Q/A (Btu/in.^{2}-sec)	Heat Transfer Coefficient h (Btu/in.^{2}-sec-°R)	Velocity V (ft/sec)
13	3	1084	78.1	1425	10	.007429	302
	4	1084	78.1	1383	10	.007665	302
14	3	1098	77.7	1182	10.21	.00924	338
	4	1098	77.7	1146	10.22	.00957	338
15	3	1102	81.2	1274	10.47	.00878	341
	4	1102	81.2	1238	10.48	.00906	341

Appendix A

TEST: D123LC-2

Data Point	Station	Pressure P_b (psi)	Temperature Bulk T_b (°R)	Temperature Wall T_i (°R)	Unit Heat Flux Q/A (Btu/in.^{2}-sec)	Heat Transfer Coefficient h (Btu/in.^{2}-sec-°R)	Velocity V (ft/sec)
1	3	1038	76.8	1549	11.25	.00764	350
	4	1038	76.8	1414	11.21	.00838	350
2	3	1039	77.1	1477	11.18	.00798	351
	4	1039	77.1	1428	11.17	.00827	351
3	3	1042	76.5	1300	10.43	.00852	344
	4	1042	76.5	1262	10.43	.0088	344
4	3	1042	76.6	1266	10.09	.00848	344
	4	1042	76.6	1216	10.10	.00887	344
5	3	1044	71.8	858	9.69	.01233	336
	4	1044	71.8	789	9.73	.01357	336
6	3	1049	73.5	1316	10.32	.00830	338
	4	1049	73.5	1249	10.33	.00879	338
7	3	1034	77.4	1649	12.69	.00808	366
	4	1034	77.4	1537	12.62	.00864	366
8	3	1033	78.4	1681	13.40	.008362	368
	4	1033	78.4	1528	13.28	.00916	368
9	3	1017	80.8	1622	13.42	.00871	389
	4	1017	80.8	1482	13.33	.00951	389

Appendix A

TEST: D123LC-3

Data Point	Station	Pressure P_b (psi)	Temperature Bulk T_b (°R)	Temperature Wall T_i (°R)	Unit Heat Flux Q/A (Btu/in.^{2}-sec)	Heat Transfer Coefficient h (Btu/in.^{2}-sec-°R)	Velocity V (ft/sec)
1	1	1086	75.5	902	7.18	.008695	220
	2	1086	75.5	883	7.19	.008907	220
	3	1079	85.3	886	7.45	.009303	254
	4	1079	85.3	958	7.41	.008496	254
2	1	1159	71.5	1046	8.44	.008666	228
	2	1159	71.5	929	8.50	.009919	228
	3	1151	82.6	1037	8.55	.008951	263
	4	1151	82.6	1033	8.55	.0090	263
3	1	1158	72.8	1151	9.15	.008485	227
	2	1158	72.8	1116	9.16	.008785	227
	3	1150	84.8	1187	9.30	.008436	267
	4	1150	84.8	1145	9.31	.008787	267
4	1	1137	70.2	991	9.16	.009952	259
	2	1137	70.2	842	9.24	.01197	259
	3	1128	80.8	979	9.32	.01038	297
	4	1128	80.8	971	9.32	.01047	297
5	1	1141	72.9	1222	10.87	.009458	258
	2	1141	72.9	1206	10.87	.009594	258
	3	1130	85	1300	10.93	.008994	305
	4	1130	85	1213	10.95	.009704	305
6	1	1125	72.6	1112	10.94	.01053	283
	2	1125	72.6	1059	10.97	.01112	283
	3	1113	84	1188	11.15	.0101	332
	4	1113	84	1136	11.17	.01062	332

Appendix A

TEST: D123LC-3

Data Point	Station	Pressure P_b (psi)	Temperature Bulk T_b (°R)	Temperature Wall T_i (°R)	Unit Heat Flux Q/A (Btu/in.^{2}-sec)	Heat Transfer Coefficient h (Btu/in.^{2}-sec-°R)	Velocity V (ft/sec)
7	1	1129	75.2	1183	11.02	.009947	283
	2	1129	75.2	1138	11.04	.01038	283
	3	1117	86.8	1252	11.00	.009437	335
	4	1117	86.8	1180	11.02	.01008	335

Appendix A

TEST: D123LC-4

Data Point	Station	Pressure P_b (psi)	Temperature Bulk T_b (°R)	Temperature Wall T_i (°R)	Unit Heat Flux Q/A (Btu/in.^{2}-sec)	Heat Transfer Coefficient h (Btu/in.^{2}-sec-°R)	Velocity V (ft/sec)
1	1	1100	70.0	986	8.11	.00885	225
	2	1100	70.0	855	8.18	.01042	225
	3	1093	80.4	992	8.11	.008889	258
	4	1093	80.4	981	8.11	.009005	258
2	1	1099	71.8	1115	8.82	.008450	225
	2	1099	71.8	1062	8.84	.008933	225
	3	1091	83.2	1161	9.05	.008404	264
	4	1091	83.2	1107	9.08	.008863	264
3	1	1101	73.4	1210	10.01	.008808	234
	2	1101	73.4	1251	10.00	.008493	234
	3	1092	85.6	1364	10.07	.007879	279
	4	1092	85.6	1236	10.09	.008772	279
4	1	1076	72.5	1183	10.84	.009767	268
	2	1076	72.5	1175	10.85	.009835	268
	3	1065	84.2	1258	10.97	.009351	318
	4	1065	84.2	1191	10.99	.009932	318
5	1	1058	73.9	1265	12.19	.01023	300
	2	1058	73.9	1309	12.18	.009867	300
	3	1044	85.6	1315	12.39	.01007	357
	4	1044	85.6	1263	12.4	.01053	357

Appendix A

TEST: D123LC-5

Data Point	Station	Pressure P_b (psi)	Temperature Bulk T_b (°R)	Temperature Wall T_i (°R)	Unit Heat Flux Q/A (Btu/in.^{2}-sec)	Heat Transfer Coefficient h (Btu/in.^{2}-sec-°R)	Velocity V (ft/sec)
1	1	1094	71.9	1109	13.21	.01274	329
	2	1094	71.9	1238	13.17	.0113	329
	3	1076	83.4	1254	13.33	.01139	388
	4	1076	83.4	1249	13.33	.01144	388
2	1	1090	74.6	1343	14.23	.01122	337
	2	1090	74.6	1383	14.24	.01089	337
	3	1071	86.7	1137	14.59	.01389	404
	4	1071	86.7	1430	14.61	.01087	404
3	1	1094	82.0	1356	14.44	.01133	359
	2	1094	82.0	1424	14.46	.01078	359
	3	1076	94.2	1540	15.33	.0106	438

TEST: D123LC-6

Data Point	Station	Pressure P_b (psi)	Temperature Bulk T_b (°R)	Temperature Wall T_i (°R)	Unit Heat Flux Q/A (Btu/in.^{2}-sec)	Heat Transfer Coefficient h (Btu/in.^{2}-sec-°R)	Velocity V (ft/sec)
1	1	1108	73.2	1041	6.48	.006697	166
	2	1108	73.2	975	6.51	.007215	166
	3	1104	84.7	1085	6.69	.006686	195
2	1	1105	78.0	1154	8.24	.007661	179
	2	1105	78.0	1213	8.22	.007243	179
	3	1099	92.0	1262	8.53	.007286	223
3	1	1105	80.0	1285	9.73	.008075	192
	2	1105	80.0	1327	9.72	.007795	192
	3	1098	95.2	1449	9.92	.007328	244
4	1	1105	80.4	1315	9.75	.0079	192
	2	1105	80.4	1312	9.76	.007923	192
	3	1098	95.8	1460	10.03	.007354	245
5	1	1098	79.1	1278	9.895	.008253	205
	2	1098	79.1	1332	9.885	.007889	205
	3	1090	93.4	1443	10.11	.007488	257
6	1	1086	79.2	1258	10.75	.009122	232
	2	1086	79.2	1449	10.74	.007840	232
	3	1077	93.1	1475	10.89	.007881	290
7	1	1064	75.9	1202	10.80	.009591	258
	2	1064	75.9	1280	10.78	.008959	258
	3	1053	88.3	1408	11.00	.008335	312
8	1	1068	78.9	1195	11.80	.01058	259
	2	1068	78.9	1519	11.81	.008199	259
	3	1057	92.4	1562	12.07	.008216	321

Appendix A

TEST: D123LC-7

Data Point	Station	Pressure P_b (psi)	Temperature Bulk T_b (°R)	Temperature Wall T_i (°R)	Unit Heat Flux Q/A (Btu/in.^{2}-sec)	Heat Transfer Coefficient h (Btu/in.^{2}-sec-°R)	Velocity V (ft/sec)
1	1	1096	72.8	973	11.68	.01297	286
	2	1096	72.8	1123	11.61	.01105	286
	3	1084	84.7	1381	11.56	.00892	340
2	1	1098	74.8	1085	12.87	.01275	288
	2	1098	74.8	1343	12.82	.01011	288
	3	1084	87.7	1571	13.06	.008809	349

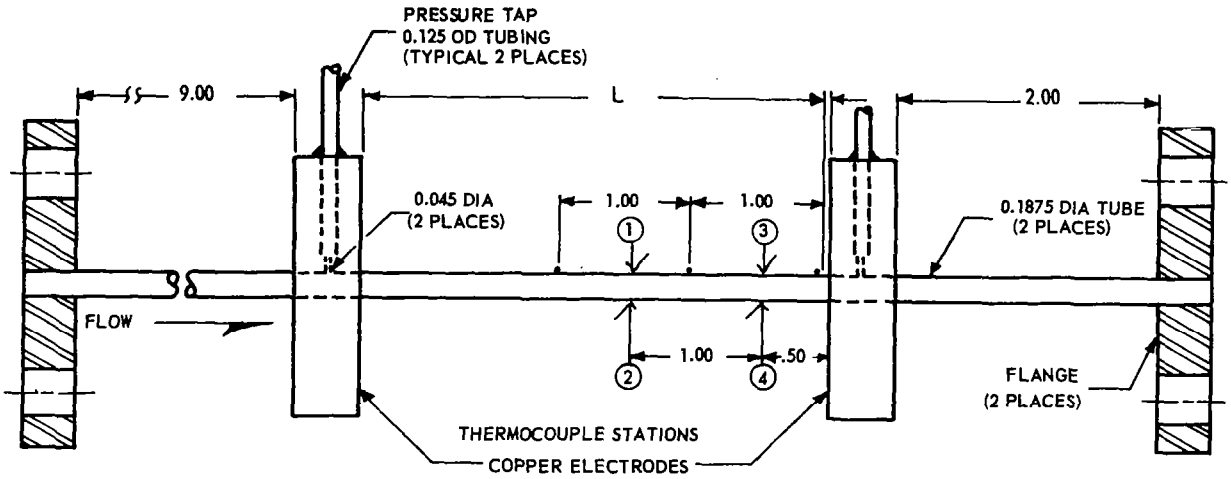

✓ CHROMEL-ALUMEL THERMOCOUPLES

• VOLTAGE TAPS

DIMENSIONS IN INCHES
TEST SECTION, HASTELLOY X TUBE
NOM. WALL THICKNESS 0.015 IN.
INSIDE DIAMETER 0.1475 IN.

TEST SECTION	L	TEST NO.
1	2.72	D 123 LC-1, -2
2	2.96	D 123 LC-3, -4, -5, -6, -7
3	3.20	D 123 LC-8, -9, -10

STRAIGHT-TUBE TEST SECTION

TEST: HT-3-104

Data Point	Station	Pressure P_b (psi)	Temperature Bulk T_b (°R)	Temperature Wall T_i (°R)	Unit Heat Flux Q/A (Btu/in.^{2}-sec)	Heat Transfer Coefficient h (Btu/in.^{2}-sec-°R)	Velocity V (ft/sec)
1	1	880	61.6	474	11.05	.0268	460
	2	880	61.6	465	11.05	.02741	460
	4	851	68.3	646	11.38	.01969	504
3	1	1273	70.3	685	14.85	.02417	431
	2	1273	70.3	704	14.85	.02344	431
	4	1245	81.1	949	15.10	.0174	493
4	1	1256	71.5	875	15.38	.01914	418
	2	1256	71.5	865	15.39	.0194	418
	4	1228	83.0	1167	15.59	.01438	485
5	1	912	65.2	526	16.91	.0367	689
	2	912	65.2	534	16.92	.03611	689
	4	847	71.7	850	17.31	.02225	769
6	1	1081	70.0	952	14.41	.01634	409
	2	1081	70.0	893	14.43	.01754	409
	4	1053	80.7	1340	14.79	.01174	475
7	1	877	66.0	786	16.09	.02234	583
	2	877	66.0	725	16.10	.02442	583
	4	825	73.3	1159	16.57	.01526	662
8	1	939	69.2	1179	14.83	.01336	426
	2	939	69.2	1109	14.83	.01427	426
	4	906	79.1	1373	15.11	.01167	502
9	1	754	65.6	1066	16.40	.01639	586
	2	754	65.6	966	16.41	.01824	586
	4	696	72.4	1286	16.75	.01380	683

Appendix A

TEST: HT-3-105

Data Point	Station	Pressure P_b (psi)	Temperature Bulk T_b (°R)	Temperature Wall T_i (°R)	Unit Heat Flux Q/A (Btu/in.^{2}-sec)	Heat Transfer Coefficient h (Btu/in.^{2}-sec-°R)	Velocity V (ft/sec)
1	1	1213	71.5	782	14.44	.02031	414
	2	1213	71.5	746	14.45	.02141	414
	4	1186	82.5	1136	14.84	.01408	478
2	1	1186	72.4	952	14.71	.01674	398
	2	1186	72.4	905	14.73	.01769	398
	4	1159	83.9	1350	15.13	.01195	467
3	1	1144	71.2	635	19.02	.03374	636
	2	1144	71.2	581	18.99	.03724	636
	4	1087	80.2	1012	19.58	.02102	725
4	1	972	70.0	581	18.95	.03711	730
	2	972	70.0	552	18.92	.03924	730
	4	896	77.0	1032	19.62	.02054	836
5	1	954	71.0	665	18.98	.03198	714
	2	954	71.0	631	18.97	.0339	714
	4	879	78.1	1138	19.64	.01853	824

Appendix A

TEST: HT-3-106

Data Point	Station	Pressure P_b (psi)	Temperature Bulk T_b (°R)	Temperature Wall T_i (°R)	Unit Heat Flux Q/A (Btu/in.^{2}-sec)	Heat Transfer Coefficient h (Btu/in.^{2}-sec-°R)	Velocity V (ft/sec)
1	4	1064	73.9	540	18.7	.04009	918
2	2	1013	68.4	452	21.38	.05575	866
	4	916	74.8	1013	22.42	.02389	979
3	1	1118	70.6	430	24.07	.06686	900
	4	1012	78.0	817	25.12	.03402	1017

Appendix A

TEST: HT-3-107

Data Point	Station	Pressure P_b (psi)	Temperature Bulk T_b (°R)	Temperature Wall T_i (°R)	Unit Heat Flux Q/A (Btu/in.^{2}-sec)	Heat Transfer Coefficient h (Btu/in.^{2}-sec-°R)	Velocity V (ft/sec)
1	1	1289	71.62	557	24.3	.05015	745
	2	1289	71.62	587	24.4	.04735	745
	3	1212	81.54	1314	25.9	.02105	856
	4	1212	81.54	1028	25.5	.02699	856
2	1	1259	71.95	690	24.6	.03987	730
	2	1259	71.95	692	24.6	.03975	730
	3	1184	81.95	1427	26.3	.01957	842
	4	1184	81.95	1150	25.8	.02417	842
3	2	1097	76.69	570	26.4	.05342	980
	3	967	83.41	1019	27.6	.02959	1138
	4	967	83.41	992	27.6	.03040	1138

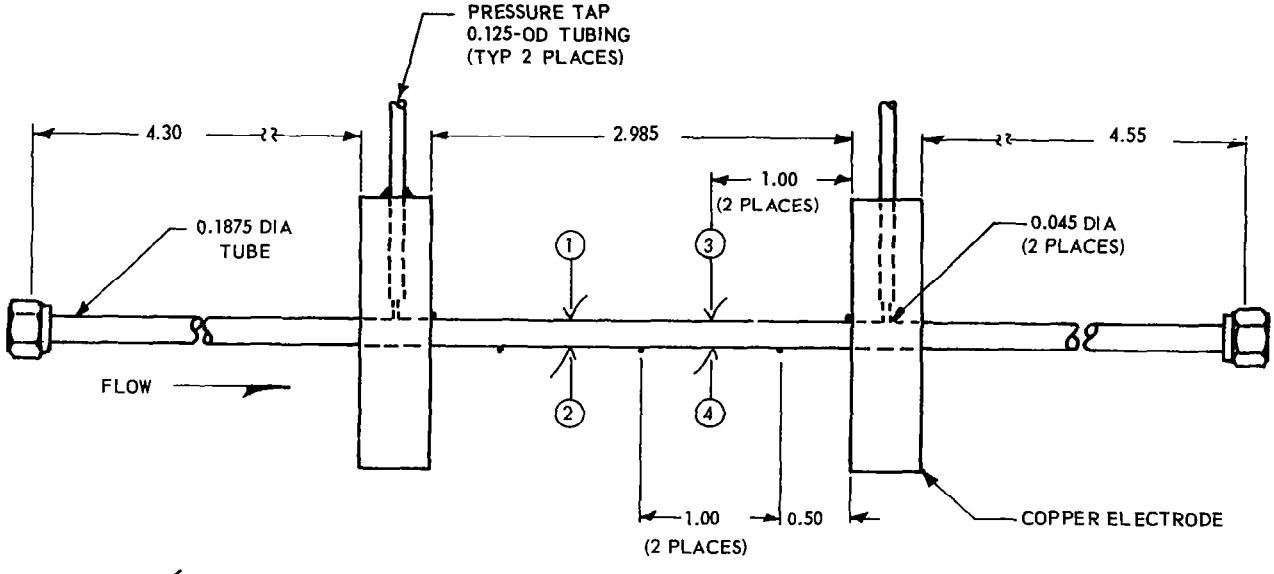

TEST HT-3-104, -105, -106, -107
STRAIGHT-TUBE TEST SECTION

Appendix A

TEST: HT-3-109

Data Point	Station	Pressure P_b (psi)	Temperature Bulk T_b (°R)	Temperature Wall T_i (°R)	Unit Heat Flux Q/A (Btu/in.^{2}-sec)	Heat Transfer Coefficient h (Btu/in.^{2}-sec-°R)	Velocity V (ft/sec)
1	1	1222	70.22	566	18.51	.03731	765
	2	1148	77.87	506	19.55	.04560	853
	3	1074	84.43	687	20.27	.03361	959
	4	1074	84.43	845	20.30	.02667	959
	5	999	90.06	1046	20.46	.02140	1080
	6	999	90.06	894	20.43	.02541	1080
	7	925	94.2	891	20.55	.02578	1244
2	1	1371	71.95	532	22.41	.04862	910
	3	1155	86.09	573	24.18	.04963	1154
	4	1155	86.09	862	24.48	.03152	1154
	5	1047	91.01	1240	24.97	.02173	1300
	6	1047	91.01	766	24.52	.03630	1300
	7	938	94.45	1134	25.14	.02418	1489

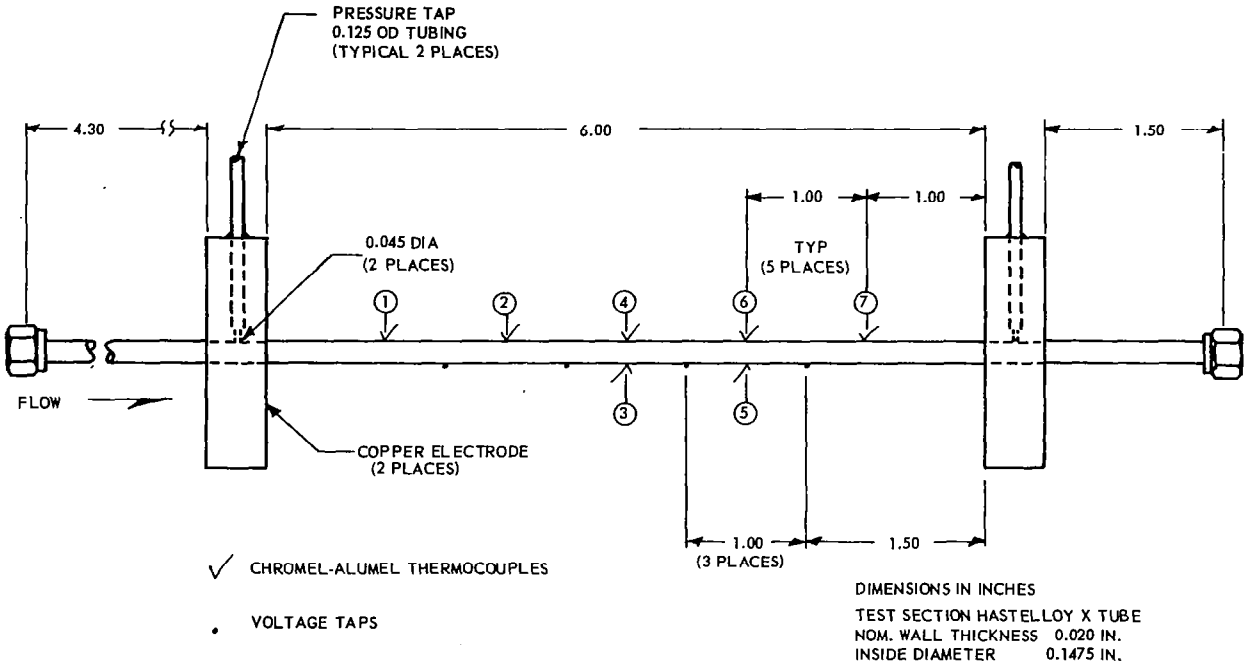

TEST HT-3-109
STRAIGHT TUBE TEST SECTION

Appendix A

TEST: HT-3-110

Data Point	Station	Pressure P_b (psi)	Temperature Bulk T_b (°R)	Temperature Wall T_i (°R)	Unit Heat Flux Q/A (Btu/in.^{2}-sec)	Heat Transfer Coefficient h (Btu/in.^{2}-sec-°R)	Velocity V (ft/sec)
1	1	1173	69.99	508	19.57	.04463	858
	4	976	82.65	1030	21.62	.02283	1080
	5	878	86.55	1333	21.92	.01758	1243
	6	878	86.55	883	21.61	.02713	1243
	7	779	89.05	1039	21.79	.02295	1433
2	1	1276	72.17	442	21.00	.05675	922
	4	1066	84.82	974	22.97	.02581	1156
	5	961	89.04	1268	23.27	.01974	1310
	6	961	89.04	724	22.88	.03601	1310
	7	856	91.54	862	23.29	.02676	1500
3	1	1265	72.87	453	20.78	.05465	912
	4	1058	85.52	999	22.77	.02492	1146
	5	954	89.67	1345	23.14	.01843	1304
	6	954	89.67	749	22.67	.03435	1304
	7	851	92.24	1048	23.08	.02416	1495

Appendix A

TEST: HT-3-111

Data Point	Station	Pressure P_b (psi)	Temperature Bulk T_b (°R)	Temperature Wall T_i (°R)	Unit Heat Flux Q/A (Btu/in.^{2}-sec)	Heat Transfer Coefficient h (Btu/in.^{2}-sec-°R)	Velocity V (ft/sec)
1	1	1312	70.03	549	19.73	.04114	786
	4	1163	85.11	989	21.44	.02371	985
	5	1088	90.89	1266	22.02	.01874	1109
	6	1088	90.89	807	21.76	.03035	1109
	7	1014	95.97	1028	21.77	.02336	1243
2	1	1295	70.14	590	19.85	.03818	767
	2	1221	78.50	501	20.87	.04931	859
	3	1221	78.50	500	20.87	.04948	859
	4	1148	85.53	1054	21.63	.02234	969
	5	1074	91.47	1459	22.40	.01638	1094
	6	1074	91.47	889	21.88	.02741	1094
	7	1001	96.78	1070	21.84	.02243	1232
3	1	1172	69.40	552	19.44	.04025	819
	2	1080	76.67	481	20.60	.05090	913
	3	1080	76.67	478	20.61	.05134	913
	4	988	82.76	1007	21.23	.02298	1031
	5	897	87.14	1524	22.14	.01541	1191
	6	897	87.14	913	21.53	.02606	1191
	7	805	90.26	1044	21.42	.02246	1362
4	4	1121	84.41	889	22.86	.02841	1138
	5	1019	89.17	1252	23.58	.02027	1272
	6	1019	89.17	618	23.10	.04364	1272
	7	917	92.30	944	23.38	.02745	1457

Appendix A

TEST: HT-3-111

Data Point	Station	Pressure P_b (psi)	Temperature Bulk T_b (°R)	Temperature Wall T_i (°R)	Unit Heat Flux Q/A (Btu/in.^{2}-sec)	Heat Transfer Coefficient h (Btu/in.^{2}-sec-°R)	Velocity V (ft/sec)
5	4	1110	85.44	937	23.00	.02699	1132
	5	1009	90.28	1405	23.95	.01821	1270
	6	1009	90.28	688	23.28	.03893	1270
	7	909	93.41	1023	23.49	.02527	1463
6	4	1102	85.80	873	22.78	.02892	1191
	5	993	90.17	1132	23.37	.02243	1335
	6	993	90.17	563	22.94	.04843	1335
	7	884	92.52	913	23.33	.02841	1534
7	4	1108	87.40	928	23.18	.02755	1181
	5	1001	91.93	1393	24.08	.01850	1325
	6	1001	91.93	639	23.37	.04270	1325
	7	893	94.51	986	23.66	.02652	1532

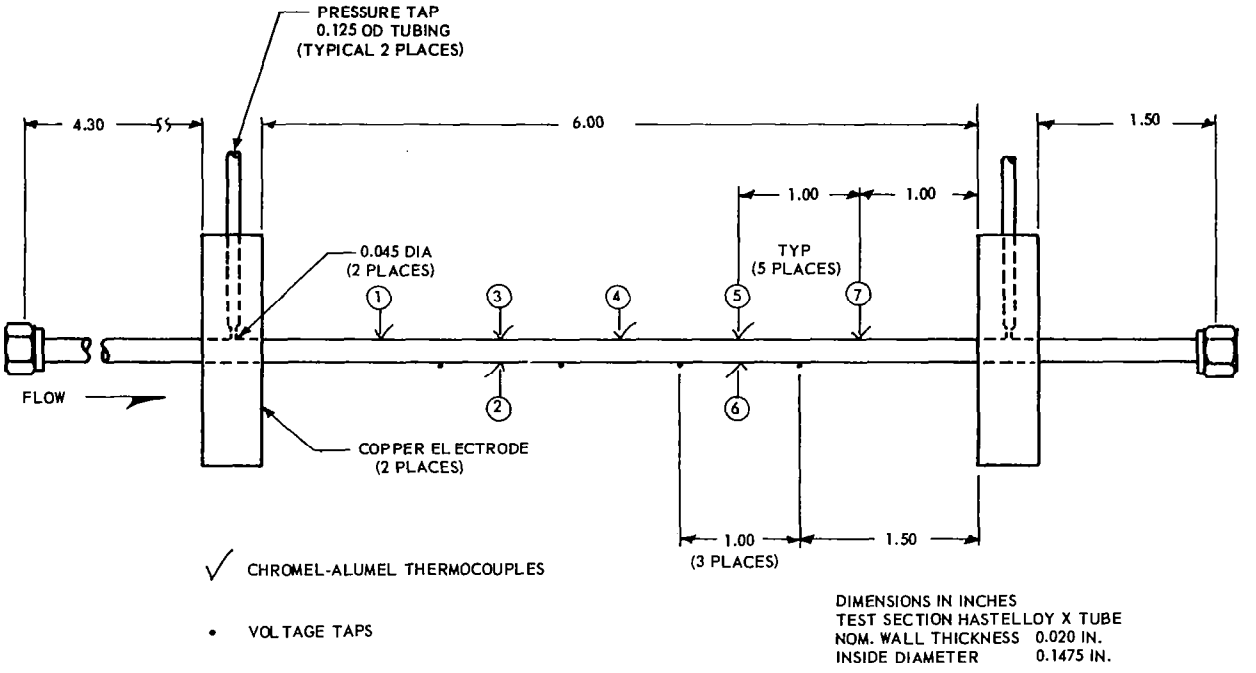

TEST HT-3-110, -111

STRAIGHT TUBE TEST SECTION

APPENDIX B

CURVED TUBE TEST DATA

Appendix B

Test No. HT-3-116 B-1-1

Pressure Inlet 1031 psia Test Section Pressure Drop 181.5 psi

Weight Flow Rate .4542 lb/sec

Input Power 53.68 Btu/sec Heat Balance -4.89 %

Thermocouple	T_o (^oR)	T_i (^oR)	T_b (^oR)	Q/A (Btu/in.^{2}-sec)	h (Btu/in.^{2}-sec-^oR)	V ft/sec
1	1479	480	65.6	8.23	0.0198	474
2	1405	284	67.8	8.46	0.0391	488
3	1463	428	69.8	8.34	0.0233	503
4	1367	195	71.9	8.52	0.0693	519
5	1353	144*	73.9	8.64	0.1234	537
6	1391	243	75.8	8.50	0.0506	556
7	1507	542	77.6	8.22	0.0177	578
8	1628	776	79.4	8.27	0.0118	600
9	1538	606	83.7	8.24	0.0158	666

* Questionable Thermocouple

Appendix B

Test No. HT-3-116 B-1-2

Pressure Inlet 1065 psia Test Section Pressure Drop 183.5 psi

Weight Flow Rate .4118 lb/sec

Input Power 63.17 Btu/sec Heat Balance -3.45 %

Thermocouple	T_o (°R)	T_i (°R)	T_b (°R)	Q/A (Btu/in.^{2}-sec)	h (Btu/in.^{2}-sec-°R)	V ft/sec
1	1630	526	68.9	9.69	0.0212	443
2	1617	499	71.6	9.65	0.0226	459
3	1753	779	74.3	9.80	0.0139	479
4	1555	362	76.9	9.79	0.0343	500
5	1554	301	79.4	10.07	0.0454	524
6	1587	388	81.8	9.96	0.0325	549
7	1917	1059	84.0	9.84	0.0101	577
8	2372*	1672	86.2	10.31	0.0650	606
9	2676*	2038	91.8	10.76	0.0553	694

*Questionable Thermocouple

Appendix B

Test No. HT-3-116 B-2-1

Pressure Inlet 1033 psia Test Section Pressure Drop 183.1 psi

Weight Flow Rate .4575 lb/sec

Input Power 53.62 Btu/sec Heat Balance -6.75 %

Thermocouple	T_o (°R)	T_i (°R)	T_b (°R)	Q/A (Btu/in.^{2}-sec)	h (Btu/in.^{2}-sec-°R)	V ft/sec
1	1478	479	65.5	8.22	0.0199	477
2	1402	257	67.7	8.54	0.0449	491
3	1456	394	69.7	8.44	0.0260	505
4	1364	234	71.8	8.28	0.0509	522
5	1349	92*	73.7	8.86	0.4686	539
6	1387	195	75.6	8.74	0.0732	559
7	1501	536	77.4	8.17	0.0178	580
8**						
9**						

*Questionable Wall Temperature
**Thermocouples Failed

Appendix B

Test No. HT-3-116 B-2-2

Pressure Inlet 1062 psia Test Section Pressure Drop 178.3 psi

Weight Flow Rate .3947 lb/sec

Input Power 63.84 Btu/sec Heat Balance -15.17 %

Thermocouple	T_o (°R)	T_i (°R)	T_b (°R)	Q/A (Btu/in.^{2}-sec)	h (Btu/in.^{2}-sec-°R)	V ft/sec
1	1301*	--	69.9	--	--	--
2	1719	683	72.8	9.96	0.0163	447
3	1949*	1081	75.6	10.10	0.0100	468
4	1616	507	78.4	9.61	0.0224	490
5	1642	473	80.9	10.11	0.0257	515
6	1658	511	83.3	10.08	0.0235	542
7	2600**	1943	85.8	10.71	0.0057	571
8	**					
9	**					

* Questionable Temperature
**Defective Thermocouple

Appendix B

Test No. HT-3-116 C-1

Pressure Inlet 1256 psia Test Section Pressure Drop 98 psi

Weight Flow Rate .2962 lb/sec

Input Power 48.91 Btu/sec Heat Balance -1.97 %

Thermocouple	T_o (°R)	T_i (°R)	T_b (°R)	Q/A (Btu/in.^{2}-sec)	h (Btu/in.^{2}-sec-°R)	V ft/sec
1	*					
2	1588	793	73.7	7.67	0.0106	323
3	1904*	1268	76.9	7.71	0.0064	337
4	1435	554	80.1	7.36	0.0155	351
5	1428	456	83.2	7.80	0.0209	367
6	1478	566	86.1	7.78	0.0162	383
7	*					
8	*					
9	*					

*Defective Thermocouple

Appendix B

Test No. HT-3-116 C-2

Pressure Inlet 1148 psia Test Section Pressure Drop 156 psi

Weight Flow Rate .3683 lb/sec

Input Power 65.25 Btu/sec Heat Balance -3.11 %

Thermocouple	T_o (°R)	T_i (°R)	T_b (°R)	Q/A (Btu/in.^{2}-sec)	h (Btu/in.^{2}-sec-°R)	V ft/sec
1	*					
2	2002	1133	74.6	10.38	0.0098	418
3	2588*	1895	77.8	11.15	0.0061	438
4	1740	736	80.9	9.90	0.0151	460
5	1755	695	83.9	10.35	0.0169	483
6	1845	862	86.7	10.42	0.0134	507
7	*					
8	*					
9	*					

*Defective Thermocouple

Appendix B

Test No. HT-3-116 C-3

Pressure Inlet 1149 psia Test Section Pressure Drop 150.3 psi

Weight Flow Rate .3205 lb/sec

Input Power 70.2 Btu/sec Heat Balance -1.88 %

Thermocouple	T_o (°R)	T_i (°R)	T_b (°R)	Q/A (Btu/in.^{2}-sec)	h (Btu/in.^{2}-sec-°R)	V ft/sec
1	*					
2	2438	1641	80.2	11.8	0.0075	393
3	3000*	2347	83.9	12.4	0.0055	417
4	1965	1026	87.6	10.8	0.0115	443
5	2060	1112	91.1	11.4	0.0112	471
6	2274	1418	94.4	11.6	0.0088	500
7	*					
8	*					
9	*					

*Defective Thermocouple

Appendix B

Test No. HT-3-118-1

Pressure Inlet 1016 psia Test Section Pressure Drop 29.9 psi

Weight Flow Rate .2184 lb/sec

Input Power 35.68 Btu/sec Heat Balance -2.45 %

Thermocouple	T_o (°R)	T_i (°R)	T_b (°R)	Q/A (Btu/in.^{2}-sec)	h (Btu/in.^{2}-sec-°R)	V ft/sec
1	1561	810	82.6	7.23	0.0099	285
2	1415	561	84.3	7.11	0.0149	293
3	1331	379	86.0	7.22	0.0246	302
4	1314	338	87.6	7.25	0.0289	310
5	1290	435	89.4	6.48	0.0187	320
6	1255	357	90.9	6.56	0.0247	329
7	1275	402	92.6	6.49	0.0210	339
8	1267	383	95.9	6.54	0.0228	359
9	1241	326	99.0	6.57	0.0289	380

Appendix B

Test No. HT-3-118-3

Pressure Inlet 1062 psia Test Section Pressure Drop 34 psi

Weight Flow Rate .205 lb/sec

Input Power 38.58 Btu/sec Heat Balance -1.07 %

Thermocouple	T_o (°R)	T_i (°R)	T_b (°R)	Q/A (Btu/in.^{2}-sec)	h (Btu/in.^{2}-sec-°R)	V ft/sec
1	1683	926	90.2	7.84	0.0093	299
2	1515	653	92.2	7.71	0.0137	309
3	1419	455	94.1	7.71	0.0213	318
4	1394	396	96.0	7.76	0.0258	329
5	1368	491	97.9	6.97	0.0177	340
6	1331	411	99.8	7.03	0.0226	351
7	1350	452	101.7	6.99	0.0199	362
8	1343	437	105.5	7.01	0.0211	384
9	1317	377	109.5	7.08	0.0264	407

Appendix B

Test No. HT-3-118-4

Pressure Inlet 1140 psia Test Section Pressure Drop 38 psi

Weight Flow Rate .2645 lb/sec

Input Power 43.84 Btu/sec Heat Balance -2.81 %

Thermocouple	T_o (°R)	T_i (°R)	T_b (°R)	Q/A (Btu/in.^{2}-sec)	h (Btu/in.^{2}-sec-°R)	V ft/sec
1	1722	859	75.4	8.84	0.0112	301
2	1565	574	77.3	8.72	0.0176	309
3	1480	376	79.3	8.84	0.0298	317
4	1464	337	81.1	8.88	0.0347	326
5	1440	461	83.0	7.91	0.0209	335
6	1404	378	84.9	8.00	0.0273	345
7	1422	420	86.7	7.94	0.0238	355
8	1417	406	90.2	7.94	0.0251	376
9	1384	327	93.6	8.04	0.0344	398

Appendix B

Test No. HT-3-118-2

Pressure Inlet 996 psia Test Section Pressure Drop 30.1 psi

Weight Flow Rate .1989 lb/sec

Input Power 37.36 Btu/sec Heat Balance -3.75 %

Thermocouple	T_o (°R)	T_i (°R)	T_b (°R)	Q/A (Btu/in.^{2}-sec)	h (Btu/in.^{2}-sec-°R)	V ft/sec
1	1675	945	85.9	7.59	0.0088	278
2	1496	654	87.9	7.49	0.0132	288
3	1404	465	89.8	7.50	0.0200	298
4	1378	406	91.6	7.53	0.0239	308
5	1352	501	93.4	6.74	0.0165	318
6	1315	421	95.3	6.81	0.0208	329
7	1334	464	97.2	6.78	0.0185	341
8	1328	451	101.0	6.78	0.0193	364
9	1305	400	104.7	6.80	0.0230	387

Appendix B

Test No. HT-3-118-5

Pressure Inlet 1110 psia Test Section Pressure Drop 37 psi

Weight Flow Rate .2259 lb/sec

Input Power 47.48 Btu/sec Heat Balance -1.08 %

Thermocouple	T_o (°R)	T_i (°R)	T_b (°R)	Q/A (Btu/in.^{2}-sec)	h (Btu/in.^{2}-sec-°R)	V ft/sec
1	1964	1143	80.8	9.75	0.00918	279
2	1725	770	83.1	9.50	0.01384	289
3	1612	542	85.5	9.40	0.02058	300
4	1585	480	87.7	9.40	0.02393	311
5	1556	580	89.9	8.58	0.01752	323
6	1518	496	92.1	8.55	0.02115	334
7	1532	529	94.2	8.56	0.01969	346
8	1531	526	98.5	8.56	0.02002	371
9	1505	467	102.8	8.59	0.02360	398

Appendix B

Test No. HT-3-118-6

Pressure Inlet 1178 psia Test Section Pressure Drop 41 psi

Weight Flow Rate .2174 lb/sec

Input Power 53.21 Btu/sec Heat Balance -1.42 %

Thermocouple	T_o (°R)	T_i (°R)	T_b (°R)	Q/A (Btu/in.^{2}-sec)	h (Btu/in.^{2}-sec-°R)	V ft/sec
1	2164	1310	86.8	11.08	0.00906	288
2	1919	950	89.4	10.75	0.01249	299
3	1750	638	92.1	10.60	0.01944	312
4	1709	548	94.7	10.53	0.02321	325
5	1673	640	97.2	9.64	0.01774	338
6	1638	567	99.8	9.59	0.02054	352
7	1655	604	102.3	9.62	0.01917	366
8	1654	601	107.5	9.62	0.01947	395
9	1631	552	112.6	9.58	0.02181	424

Appendix B

Test No. HT-3-118-7

Pressure Inlet 1116 psia Test Section Pressure Drop 37 psi

Weight Flow Rate .2224 lb/sec

Input Power 46.27 Btu/sec Heat Balance -2.23 %

Thermocouple	T_o (°R)	T_i (°R)	T_b (°R)	Q/A (Btu/in.^{2}-sec)	h (Btu/in.^{2}-sec-°R)	V ft/sec
1	2013	1250	82.4	9.44	0.00808	281
2	1785	903	84.7	9.33	0.01141	291
3	1597	547	86.9	9.22	0.02002	302
4	1559	459	89.1	9.24	0.02499	312
5	1526	560	91.3	8.34	0.01777	324
6	1494	490	93.5	8.32	0.02096	336
7	1508	522	95.6	8.32	0.01953	348
8	1508	520	99.9	8.32	0.01979	373
9	1483	464	104.1	8.36	0.02324	398

Appendix B

Test No. HT-3-118-8

Pressure Inlet 1061 psia Test Section Pressure Drop 35 psi

Weight Flow Rate .224 lb/sec

Input Power 41.39 Btu/sec Heat Balance -3.04 %

Thermocouple	T_o (°R)	T_i (°R)	T_b (°R)	Q/A (Btu/in.^{2}-sec)	h (Btu/in.^{2}-sec-°R)	V ft/sec
1	1868	1152	79.8	8.34	0.00777	277
2	1678	859	81.9	8.30	0.01068	285
3	1482	482	83.9	8.25	0.02072	295
4	1451	410	85.8	8.31	0.02562	304
5	1423	510	87.7	7.45	0.01766	314
6	1391	438	89.7	7.50	0.02150	324
7	1406	473	91.6	7.49	0.01963	335
8	1403	465	95.3	7.49	0.02027	357
9	1379	412	99.0	7.53	0.02407	380

Appendix B

Test No. HT-3-118-9

Pressure Inlet 1190 psia Test Section Pressure Drop 38 psi

Weight Flow Rate .2682 lb/sec

Input Power 38.73 Btu/sec Heat Balance -2.02 %

Thermocouple	T_o (°R)	T_i (°R)	T_b (°R)	Q/A (Btu/in.^{2}-sec)	h (Btu/in.^{2}-sec-°R)	V ft/sec
1	1546	728	80.8	7.62	0.01178	324
2	1560	735	82.5	7.73	0.01185	332
3	1389	382	84.1	7.80	0.02618	340
4	1355	298	85.8	7.86	0.03697	349
5	1327	399	87.4	7.04	0.02253	357
6	1297	328	89.0	7.12	0.02975	366
7	1309	358	90.5	7.12	0.02659	375
8	1302	341	93.6	7.12	0.02875	394
9	1269	262	96.6	7.12	0.04294	412

Appendix B

Test No. HT-3-118-10

Pressure Inlet 977 psia Test Section Pressure Drop 69.2 psi

Weight Flow Rate .3339 lb/sec

Input Power 51.91 Btu/sec Heat Balance -6.29 %

Thermocouple	T_o (°R)	T_i (°R)	T_b (°R)	Q/A (Btu/in.^{2}-sec)	h (Btu/in.^{2}-sec-°R)	V ft/sec
1	1975	1091	72.5	10.37	0.01018	384
2	1805	795	74.3	10.35	0.01435	394
3	1626	412	76.0	10.27	0.03055	406
4	1597	335	77.6	10.43	0.04046	417
5	1571	463	79.2	9.36	0.02439	429
6	1540	385	80.8	9.44	0.03102	441
7	1560	437	82.3	9.37	0.02644	455
8	1559	433	85.4	9.38	0.02696	483
9	1524	345	88.2	9.53	0.03708	513

Appendix B

Test No. HT-3-118-11

Pressure Inlet 978 psia Test Section Pressure Drop 71.5 psi

Weight Flow Rate .3001 lb/sec

Input Power 56.9 Btu/sec Heat Balance -4.57 %

Thermocouple	T_o (°R)	T_i (°R)	T_b (°R)	Q/A (Btu/in.^{2}-sec)	h (Btu/in.^{2}-sec-°R)	V ft/sec
1	2213	1331	76.4	11.61	0.00925	366
2	2025	1033	78.4	11.57	0.01212	379
3	1772	558	80.4	11.25	0.02353	392
4	1719	429	82.3	11.27	0.03252	407
5	1686	549	84.2	10.24	0.02200	422
6	1653	474	86.0	10.24	0.02639	437
7	1674	523	87.8	10.22	0.02345	453
8	1678	533	91.4	10.23	0.02317	487
9	1654	475	94.9	10.24	0.02694	523

Appendix B

Test No. HT-3-118-12

Pressure Inlet 964.8 psia Test Section Pressure Drop 72.5 psi

Weight Flow Rate .2719 lb/sec

Input Power 59.98 Btu/sec Heat Balance -4.38 %

Thermocouple	T_o (°R)	T_i (°R)	T_b (°R)	Q/A (Btu/in.^{2}-sec)	h (Btu/in.^{2}-sec-°R)	V ft/sec
1	2460	1603	79.7	12.61	0.00828	353
2	2107	1088	81.9	12.30	0.01222	367
3	1894	714	84.0	12.03	0.01909	383
4	1812	535	86.2	11.84	0.02636	400
5	1765	622	88.4	10.88	0.02039	417
6	1733	549	90.4	10.81	0.02354	435
7	1752	594	92.5	10.86	0.02166	459
8	1764	618	96.6	10.88	0.02087	493
9	1741	568	100.8	10.83	0.02314	533

Appendix B

Test No. HT-3-118-13

Pressure Inlet 1160 psia Test Section Pressure Drop 82 psi

Weight Flow Rate .3829 lb/sec

Input Power 59.83 Btu/sec Heat Balance -6.42 %

Thermocouple	T_o (°R)	T_i (°R)	T_b (°R)	Q/A (Btu/in.^{2}-sec)	h (Btu/in.^{2}-sec-°R)	V ft/sec
1	2055	1068	76.3	11.70	0.01180	441
2	1780	483	78.1	11.68	0.02884	452
3	1746	396	79.9	11.80	0.03734	464
4	1717	315	81.6	11.97	0.05123	476
5	1685	445	83.4	10.77	0.0298	489
6	1660	379	85.0	10.89	0.03699	502
7	1674	417	86.6	10.80	0.03271	516
8	1668	402	89.8	10.82	0.0346	544
9	1623	279	92.9	10.97	0.05897	574

Appendix B

Test No. HT-3-118-14

Pressure Inlet 1118 psia Test Section Pressure Drop 97 psi

Weight Flow Rate .3684 lb.sec

Input Power 64.8 Btu/sec Heat Balance -4.82 %

Thermocouple	T_o (^oR)	T_i (^oR)	T_b (^oR)	Q/A (Btu/in.^{2}-sec)	h (Btu/in.^{2}-sec-^oR)	V ft/sec
1	2228	1217	79.4	12.95	0.01138	449
2	1906	598	81.4	12.78	0.02475	463
3	1861	491	83.3	12.63	0.03100	476
4	1819	378	85.0	12.84	0.04380	491
5	1780	499	86.9	11.57	0.02810	506
6	1750	423	88.6	11.68	0.03495	522
7	1765	462	90.4	11.64	0.03129	538
8	1764	459	93.9	11.64	0.03188	571
9	1716	330	97.2	11.89	0.05100	606

Appendix B

Test No. HT-3-119-1

Pressure Inlet 1092 psia Test Section Pressure Drop 70 psi

Weight Flow Rate 0.246 lb/sec

Input Power 40.18 Btu/sec Heat Balance -1.8 %

Thermocouple	T_o (°R)	T_i (°R)	T_b (°R)	Q/A (Btu/in.^{2}-sec)	h (Btu/in.^{2}-sec-°R)	V ft/sec
1	1637	793	86.7	8.51	0.0120	368
2	1436	502	88.5	7.84	0.0189	380
3	1349	298	90.2	8.02	0.0386	391
4	1395	408	92.0	7.92	0.0250	404
5	1364	307	93.7	8.15	0.0382	416
6	1341	249	95.5	8.15	0.0531	428
7	1371	322	97.2	8.15	0.0362	441
8	1401	440	100.6	7.81	0.0230	467
9	1383	398	104.1	7.84	0.0267	495

Appendix B

Test No. HT-3-119-2

Pressure Inlet 1151 psia Test Section Pressure Drop 76 psi

Weight Flow Rate 0.271 lb/sec

Input Power 49.25 Btu/sec Heat Balance -3.4 %

Thermocouple	T_o (°R)	T_i (°R)	T_b (°R)	Q/A (Btu/in.^{2}-sec)	h (Btu/in.^{2}-sec-°R)	V ft/sec
1	1883	960	81.2	10.49	0.0119	366
2	1614	566	83.4	9.58	0.0198	379
3	1513	321	85.5	9.77	0.0414	391
4	1575	478	87.6	9.57	0.0245	405
5	1529	321	89.5	9.97	0.0430	418
6	1509	267	91.6	9.96	0.0566	432
7	1539	347	93.5	9.97	0.0392	447
8	1576	497	97.4	9.46	0.0237	477
9	1556	450	101.2	9.51	0.0272	508

Appendix B

Test No. HT-3-102-1

Pressure Inlet 1142 psia Test Section Pressure Drop 63 psi

Weight Flow Rate .298 lb/sec

Input Power 36.95 Btu/sec Heat Balance -4.5 %

Thermocouple	T_o (°R)	T_i (°R)	T_b (°R)	Q/A (Btu/in.^{2}-sec)	h (Btu/in.^{2}-sec-°R)	V ft/sec
1	1466	604	70.7	7.67	0.0144	350
2	1333	406	72.3	7.27	0.0218	357
3	1257	224	73.8	7.43	0.0492	364
4	1296	320	75.5	7.36	0.0300	372
5	1269	197	76.9	7.70	0.0642	380
6	1258	168	78.5	7.70	0.0862	389
7	1282	228	80.0	7.67	0.0517	397
8	1337	449	82.9	7.08	0.0193	415
9	1297	357	85.8	7.19	0.0264	435

Appendix B

Test No. HT-3-120-2

Pressure Inlet 1230 psia Test Section Pressure Drop 62 psi

Weight Flow Rate .265 lb/sec

Input Power 43.26 Btu/sec Heat Balance -2.0 %

Thermocouple	T_o (°R)	T_i (°R)	T_b (°R)	Q/A (Btu/in.^{2}-sec)	h (Btu/in.^{2}-sec-°R)	V ft/sec
1	1729	872	77.2	9.10	0.0114	332
2	1509	548	79.3	8.44	0.0180	341
3	1403	299	81.5	8.61	0.0396	351
4	1450	415	83.4	8.50	0.0256	361
5	1420	278	85.4	8.89	0.0462	372
6	1404	236	87.3	8.94	0.0601	382
7	1430	304	89.2	8.89	0.0415	394
8	1503	573	92.9	8.24	0.0172	418
9	1450	458	96.5	8.26	0.0228	442

Appendix B

Test No. HT-3-120-3

Pressure Inlet 1222 psia Test Section Pressure Drop 60 psi

Weight Flow Rate .226 lb/sec

Input Power 48.77 Btu/sec Heat Balance -0.7 %

Thermocouple	T_o ($^\circ$R)	T_i ($^\circ$R)	T_b ($^\circ$R	Q/A (Btu/in.^{2}-sec)	h (Btu/in.^{2}-sec-$^\circ$R)	V ft/sec
1	1880	963	84.6	10.42	0.0118	312
2	1724	786	87.2	9.66	0.0138	324
3	1561	448	89.7	9.58	0.0266	338
4	1606	552	92.1	9.55	0.0207	350
5	1569	417	94.6	9.85	0.0305	364
6	1547	361	97.0	9.98	0.0377	378
7	1574	430	99.4	9.84	0.0297	392
8	1649	686	104.2	9.36	0.0160	422
9	1612	612	109.0	9.33	0.0185	452

Appendix B

Test No. HT-3-120-4

Pressure Inlet 1034 psia Test Section Pressure Drop 121.4 psi

Weight Flow Rate .331 lb/sec

Input Power 57.72 Btu/sec Heat Balance -4.5 %

Thermocouple	T_o (°R)	T_i (°R)	T_b (°R)	Q/A (Btu/in.^{2}-sec)	h (Btu/in.^{2}-sec-°R)	V ft/sec
1	1868	700	77.4	12.09	0.0194	442
2	1991	1023	79.4	11.50	0.0122	456
3	1686	422	81.2	11.22	0.0329	472
4	1752	580	83.2	11.22	0.0226	489
5	1728	449	84.9	11.58	0.0318	507
6	1688	343	86.6	11.82	0.0461	526
7	1730	454	88.4	11.58	0.0316	546
8	1774	668	91.8	11.04	0.0191	586
9	1744	606	95.1	11.00	0.0215	629

Appendix B

Test No. HT-3-120-5

Pressure Inlet 1225 psia Test Section Pressure Drop 144 psi

Weight Flow Rate .387 lb/sec

Input Power 60.69 Btu/sec Heat Balance -4.6 %

Thermocouple	T_o (°R)	T_i (°R)	T_b (°R)	Q/A (Btu/in.^{2}-sec)	h (Btu/in.^{2}-sec-°R)	V ft/sec
1	1887	662	81.4	12.56	0.0216	518
2	1941	867	83.4	12.00	0.0153	532
3	1712	372	85.2	11.89	0.0413	548
4	1786	558	86.8	11.74	0.0249	564
5	1792	502	88.6	12.04	0.0291	580
6	1722	317	90.3	12.36	0.0544	598
7	1786	488	91.9	12.06	0.0304	615
8	1797	626	95.2	11.57	0.0218	651
9	1740	496	98.4	11.43	0.0287	689

Appendix B

Test No, HT-3-120-6

Pressure Inlet 1226 psia Test Section Pressure Drop 143 psi

Weight Flow Rate .385 lb/sec

Input Power 60.74 Btu/sec Heat Balance -4.7 %

Thermocouple	T_o (°R)	T_i (°R)	T_b (°R)	Q/A (Btu/in.^{2}-sec)	h (Btu/in.^{2}-sec-°R)	V ft/sec
1	1890	665	81.8	12.59	0.0216	517
2	1947	870	83.6	12.07	0.0153	532
3	1717	374	85.4	11.94	0.0413	548
4	1792	562	87.2	11.80	0.0248	564
5	1800	518	88.9	12.08	0.0281	580
6	1727	327	90.6	12.38	0.0522	597
7	1793	501	92.3	12.06	0.0294	615
8	1799	630	95.5	11.58	0.0216	650
9	1742	501	98.7	11.43	0.0284	688

Appendix B

Test No. HT-3-120-7

Pressure Inlet 1241 psia

Test Section Pressure Drop 61 psi

Weight Flow Rate .224 lb/sec

Input Power 45.67 Btu/sec

Heat Balance -1.2 %

Thermocouple	T_o (^oR)	T_i (^oR)	T_b (^oR)	Q/A (Btu/in.^{2}-sec)	h (Btu/in.^{2}-sec-^oR)	V ft/sec
1	1850	1001	83.2	9.69	0.0105	302
2	1708	844	85.7	9.04	0.0119	314
3	1507	444	88.2	8.98	0.0252	325
4	1559	562	90.5	8.95	0.0190	337
5	1554	509	92.8	9.14	0.0219	349
6	1495	368	95.2	9.32	0.0342	362
7	1546	491	97.4	9.15	0.0232	375
8	1589	666	102.0	8.74	0.0154	402
9	1541	569	106.5	8.70	0.0188	430

Appendix B

Test No. HT-3-120-8

Pressure Inlet 1069 psia Test Section Pressure Drop 117.3 psi

Weight Flow Rate .296 lb/sec

Input Power 61.1 Btu/sec Heat Balance -3.1 %

Thermocouple	T_o (°R)	T_i (°R)	T_b (°R)	Q/A (Btu/in.^{2}-sec)	h (Btu/in.^{2}-sec-°R)	V ft/sec
1	*					
2	*					
3	1880	735	85.8	12.05	0.0186	444
4	1933	835	88.0	12.12	0.0162	462
5	1975	859	90.2	12.54	0.0163	482
6	1837	583	92.2	12.29	0.0250	501
7	1947	808	94.3	12.50	0.0175	522
8	1897	803	98.4	11.85	0.0168	567
9	1853	718	102.5	11.79	0.0191	613

*Defective Wall Thermocouple

Appendix B

Test No. HT-3-120-9

Pressure Inlet 1054 psia Test Section Pressure Drop 115.2 psi

Weight Flow Rate .279 lb/sec

Input Power 62.2 Btu/sec Heat Balance -2.6 %

Thermocouple	T_o (°R)	T_i (°R)	T_b (°R)	Q/A (Btu/in.^{2}-sec)	h (Btu/in.^{2}-sec-°R)	V ft/sec
1	*					
2	*					
3	2074	1045	88.0	12.53	0.0131	440
4	2047	1001	90.4	12.50	0.0137	460
5	2117	1071	92.6	12.95	0.0132	481
6	1915	714	94.8	12.65	0.0204	502
7	2071	997	97.1	12.88	0.0143	526
8	1965	896	101.6	12.14	0.0152	572
9	1926	826	106.0	12.09	0.0168	622

*Defective Wall Thermocouple

Appendix B

Test No. HT-3-120-10

Pressure Inlet 1013 psia Test Section Pressure Drop 110.9 psi

Weight Flow Rate .283 lb/sec

Input Power 57.26 Btu/sec Heat Balance -3.1 %

Thermocouple	T_o (°R)	T_i (°R)	T_b (°R)	Q/A (Btu/in.^{2}-sec)	h (Btu/in.^{2}-sec-°R)	V ft/sec
1	*					
2	*					
3	1956	969	85.2	11.44	0.0129	436
4	1907	886	87.2	11.39	0.0142	455
5	1969	946	89.2	11.81	0.0138	474
6	1786	598	91.2	11.57	0.0228	494
7	1949	912	93.2	11.79	0.0144	515
8	1850	824	97.2	11.06	0.0152	559
9	1811	752	101.2	11.02	0.0169	605

*Defective Wall Thermocouple

Appendix B

Test No. HT-3-120-11

Pressure Inlet 972 psia Test Section Pressure Drop 106.5 psi

Weight Flow Rate .292 lb/sec

Input Power 51.53 Btu/sec Heat Balance -3.7 %

Thermocouple	T_o (°R)	T_i (°R)	T_b (°R)	Q/A (Btu/in.^{2}-sec)	h (Btu/in.^{2}-sec-°R)	V ft/sec
1	*					
2	*					
3	1751	767	81.7	10.13	0.0148	434
4	1738	743	83.6	10.13	0.0154	450
5	1772	759	85.3	10.46	0.0155	468
6	1640	482	87.0	10.31	0.0261	485
7	1779	772	88.8	10.47	0.0153	504
8	1704	708	92.1	9.91	0.0160	542
9	1670	640	95.4	9.88	0.0181	584

*Defective Wall Thermocouple

Appendix B

Test No. HT-3-121-1

Pressure Inlet 1259 psia Test Section Pressure Drop 51 psi

Weight Flow Rate .202 lb/sec

Input Power 42.75 Btu/sec Heat Balance -1.0 %

Thermocouple	T_o (°R)	T_i (°R)	T_b (°R)	Q/A (Btu/in.^{2}-sec)	h (Btu/in.^{2}-sec-°R)	V ft/sec
1	1635	953	79.6	7.24	0.0083	258
2	1571	605	85.9	8.88	0.0171	280
3	1602	667	87.9	8.89	0.0154	289
4	1559	573	91.8	8.89	0.0184	306
5	1588	633	95.6	8.92	0.0166	324
6	1639	630	99.4	9.57	0.0180	342
7	1943	1144*	104.9	9.72	0.0094	372
8	1394	406	110.4	7.92	0.0268	402
9	1438	506	114.1	7.84	0.0200	422

*Defective Wall Thermocouple

Appendix B

Test No. HT-3-121-2

Pressure Inlet 1200 psia Test Section Pressure Drop 60 psi

Weight Flow Rate .205 lb/sec

Input Power 45.95 Btu/sec Heat Balance -0.6 %

Thermocouple	T_o (°R)	T_i (°R)	T_b (°R)	Q/A (Btu/in.^{2}-sec)	h (Btu/in.^{2}-sec-°R)	V ft/sec
1	1693	972	81.5	7.83	0.0088	272
2	1701	753	87.8	9.58	0.0144	298
3	1689	732	89.8	9.58	0.0149	308
4	1646	638	93.8	9.59	0.0176	328
5	1697	738	97.7	9.63	0.0150	349
6	1708	651	101.5	10.30	0.0188	370
7	2064*	1242	107.3	10.57	0.0093	404
8	1473	469	113.2	8.46	0.0238	438
9	1518	566	117.1	8.45	0.0188	462

*Defective Wall Thermocouple

Appendix B

Test No. HT-3-121-3

Pressure Inlet 1155 psia Test Section Pressure Drop 65 psi

Weight Flow Rate .199 lb/sec

Input Power 48.50 Btu/sec Heat Balance -0.7 %

Thermocouple	T_o (°R)	T_i (°R)	T_b (°R)	Q/A (Btu/in.^{2}-sec)	h (Btu/in.^{2}-sec-°R)	V ft/sec
1	*					
2	1803	865	91.6	10.14	0.0131	314
3	1777	818	93.8	10.12	0.0139	325
4	1717	696	97.9	10.14	0.0169	348
5	1755	770	102.0	10.17	0.0152	371
6	1773	692	106.2	10.89	0.0186	395
7	2437*	1677	112.5	11.68	0.0074	433
8	1541	529	118.9	8.90	0.0217	472
9	1589	630	123.3	8.96	0.0176	498

*Defective Wall Thermocouple

Appendix B

Test No. HT-3-121-4

Pressure Inlet 1153 psia Test Section Pressure Drop 65 psi

Weight Flow Rate .197 lb/sec

Input Power 48.57 Btu/sec Heat Balance -0.6 %

Thermocouple	T_o (°R)	T_i (°R)	T_b (°R)	Q/A (Btu/in.^{2}-sec)	h (Btu/in.^{2}-sec-°R)	V ft/sec
1	*					
2	1815	882	92.2	10.17	0.0129	314
3	1784	828	94.4	10.15	0.0138	325
4	1722	707	98.6	10.15	0.0166	348
5	1761	780	102.8	10.17	0.0150	372
6	1780	704	107.1	10.91	0.0182	396
7	2511*	1769	113.5	11.82	0.0016	434
8	1545	534	119.9	8.92	0.0216	473
9	1594	636	124.4	8.98	0.0176	500

*Defective Wall Thermocouple

Appendix B

Test No. HT-3-121-5

Pressure Inlet 1251 psia Test Section Pressure Drop 63 psi

Weight Flow Rate .224 lb/sec

Input Power 48.93 Btu/sec Heat Balance -0.8 %

Thermocouple	T_o (°R)	T_i (°R)	T_b (°R)	Q/A (Btu/in.^{2}-sec)	h (Btu/in.^{2}-sec-°R)	V ft/sec
1	1511	584	79.1	8.28	0.0164	284
2	1703	670	85.6	10.12	0.0173	310
3	1727	719	87.6	10.14	0.0160	320
4	1674	592	91.6	10.20	0.0204	340
5	1710	666	95.5	10.24	0.0179	360
6	1734	596	99.3	10.92	0.0220	382
7	2341*	1548	105.0	11.62	0.0080	416
8	1508	447	110.7	8.97	0.0266	450
9	1558	561	114.4	8.95	0.0200	474

*Defective Wall Thermocouple

Appendix B

Test No. HT-3-121-6

Pressure Inlet 1241 psia Test Section Pressure Drop 63 psi

Weight Flow Rate .199 lb/sec

Input Power 53.26 Btu/sec Heat Balance -0.4 %

Thermocouple	T_o (°R)	T_i (°R)	T_b (°R)	Q/A (Btu/in.^{2}-sec)	h (Btu/in.^{2}-sec-°R)	V ft/sec
1	*					
2	1924	946	91.8	11.17	0.0130	303
3	1923	945	94.2	11.17	0.0131	314
4	1857	809	98.9	11.26	0.0159	338
5	1916	913	103.6	11.32	0.0139	362
6	1939	854	108.2	12.07	0.0162	386
7	*					
8	1644	606	122.5	9.76	0.0202	465
9	1701	719	127.3	9.80	0.0166	492

*Defective Wall Thermocouple

Appendix B

Test No. HT-3-121-7

Pressure Inlet 1197 psia Test Section Pressure Drop 72 psi

Weight Flow Rate .223 lb/sec

Input Power 53.25 Btu/sec Heat Balance -1.7 %

Thermocouple	T_o (°R)	T_i (°R)	T_b (°R)	Q/A (Btu/in.^{2}-sec)	h (Btu/in.^{2}-sec-°R)	V ft/sec
1	*					
2	1978	1035	87.7	11.21	0.0118	326
3	1925	949	89.9	11.16	0.0130	337
4	1889	871	94.0	11.25	0.0144	360
5	1944	965	98.2	11.30	0.0130	384
6	1943	862	102.2	12.07	0.0158	409
7	*					
8	1621	556	114.6	9.72	0.0220	489
9	1669	656	118.7	9.78	0.0182	517

*Defective Wall Thermocouple

Appendix B

Test No. HT-3-121-8

Pressure Inlet 1167 psia Test Section Pressure Drop 74 psi

Weight Flow Rate .214 lb/sec

Input Power 54.46 Btu/sec Heat Balance -1.0 %

Thermocouple	T_o (°R)	T_i (°R)	T_b (°R)	Q/A (Btu/in.^{2}-sec)	h (Btu/in.^{2}-sec-°R)	V ft/sec
1	*					
2	2077	1159	90.2	11.56	0.0108	329
3	2005	1049	92.4	11.48	0.0120	342
4	2019	1054	96.8	11.65	0.0122	366
5	2000	1024	101.1	11.63	0.0126	392
6	1998	924	105.4	12.40	0.0152	420
7	*					
8	1655	588	118.6	9.98	0.0212	505
9	1700	680	123.0	10.03	0.0179	534

*Defective Wall Thermocouple

Appendix B

Test No. HT-3-121-9

Pressure Inlet 1194 psia Test Section Pressure Drop 76 psi

Weight Flow Rate .218 lb/sec

Input Power 54.95 Btu/sec Heat Balance -1.2 %

Thermocouple	T_o (°R)	T_i (°R)	T_b (°R)	Q/A (Btu/in.^{2}-sec)	h (Btu/in.^{2}-sec-°R)	V ft/sec
1	*					
2	2160	1269	92.0	11.76	0.0099	340
3	2059	1121	94.3	11.63	0.0113	352
4	2152	1243	98.6	11.90	0.0104	378
5	2007	1023	102.9	11.73	0.0128	404
6	2003	918	107.3	12.51	0.0154	431
7	*					
8	1657	716	120.5	9.27	0.0156	516
9	1697	790	124.9	9.28	0.0139	545

*Defective Wall Thermocouple

Appendix B

Test No. HT-3-121-10

Pressure Inlet 1193 psia Test Section Pressure Drop 74 psi

Weight Flow Rate .210 lb/sec

Input Power 55.02 Btu/sec Heat Balance -0.4 %

Thermocouple	T_o (°R)	T_i (°R)	T_b (°R)	Q/A (Btu/in.^{2}-sec)	h (Btu/in.^{2}-sec-°R)	V ft/sec
1	*					
2	2199	1324	96.0	11.80	0.0096	349
3	2097	1179	98.2	11.67	0.0108	362
4	2229	1348	102.8	12.03	0.0096	388
5	2009	1024	107.2	11.75	0.0128	415
6	2001	912	111.7	12.53	0.0156	442
7	*					
8	1662	585	125.6	10.07	0.0219	529
9	1700	666	130.3	10.12	0.0189	558

*Defective Wall Thermocouple